4 Sampling the band structure

In two-photon photoemission (2PPE) an electron is excited from the initial state to the intermediate state and subsequently to the final state, with both transitions being mediated by photons. The peaks in the spectrum usually relate directly to the intermediate states, their intensity, however, strongly depends on the initial-state distribution and the transition matrix elements. This is explicitly demonstrated in spin-resolved measurements and vice versa used to study the electronic structure of the initial states close to the Fermi level. What is more, magnetic linear dichroism can be observed in energy- and time-resolved measurements. Dichroism is related to a hybridization of the initial states due to spin-orbit coupling. The explicit use of spin resolution but also of spin-integrated time-resolved measurements allows us to determine of the relativistic quantum numbers of the initial states.

4.1 Two-photon photoemission of image-potential states

4.1.1 Spin-integrated spectroscopy

To get familiar with the typical features in energy resolved 2PPE, we start this chapter with a spectrum of Cu(100) shown in Figure 4.1. The low energy cut-off at zero kinetic energy stems from electrons directly excited with the ultraviolet pump pulse. This is possible since the work function of Cu(100) ($\phi = E_{vac} - E_F = 4.62$ eV) is slightly smaller than the pump-pulse photon energy ($h\nu_{pump} = 4.67$ eV). The initial-state energy of the electrons from the cut-off is therefore close to the Fermi level. The intensity of the peak considerably decreases with decreasing pump-pulse photon energy or with increasing work function. The peaks at 1 eV and 1.4 eV kinetic energy are related to the $n=1$ and $n=2$ image-potential states. The image-potential states with $n \geq 3$ are visible as a shoulder at the high energy side of the $n=2$ state.

The intensity distribution of the image-potential states in a 2PPE spectrum, which can be described by the optical Bloch equations (see 2.2.2), is influenced by three factors:

- Initial density of states: For several initial states the spectral distribution

is determined by a weighted sum over these states. Considering bulk states in Cu(100) the initial-state distribution, i.e. the bulk sp bands, is almost constant in the significant energy range ($E - E_F$ <0.8 eV). This, however, does not hold for iron and cobalt due to the significantly structured d-density of states in this energy range.

- Transition matrix elements of the pump and probe processes: With the respective initial and final states ψ_i and ψ_j the matrix element is $< \psi_j|\hat{\mu}|\psi_i >$. The dipole operator $\hat{\mu}$ is expressed as the product of the vector potential with the momentum operator ($\vec{A} \cdot \vec{p}$), which is derived from first order perturbation theory and neglecting the $\nabla\vec{A}$ term (see e.g. [*Matzdorf*, 1998]). On one hand the transition-matrix elements depend on the symmetry of the initial, intermediate, and final state in combination with the light polarization. The dipole selection rules have already been discussed in Section 2.3.2. On the other hand the matrix elements scale with the overlap of the image-potential-state wave-function with the initial states. For initial states with bulk character the transition matrix elements are proportional to the overlap of the image-potential-state wave-function with the bulk. This leads to a proportionality of the transition matrix elements to $(n+a)^{-3/2}$ [*Klamroth et al.*, 2001]. Note that these elements enter quadratically in the intensity of the pump and probe processes, which should together lead to a $(n+a)^{-6}$ dependence in the spectrum. Initial states with surface character may significantly modify this intensity dependence.

- Decay and dephasing: Due to the finite lifetime of the intermediate state, the rise in population, which is caused by the pump pulse is followed by an exponential decay. As discussed in Section 2.1.2 the lifetime depends on the quantum number of the image-potential states. The $n=2$ and $n=3$ states become enhanced and even dominant for large pump-probe delay. The spin dependence of the lifetime leads to a time-dependent spin polarization. Dephasing , i.e. quasielastic scattering events, adds to the linewidth. Moreover, this contribution depends on the delay between pump and probe pulses. Details can be found in [*Boger et al.*, 2002].

In the proceeding text, the effects of inelastic decay and dephasing on the intensity of the image-potential states will be neglected. This is justified by the following consideration: We are only interested in the spin polarization of a image-potential state and not in the intensity ratio between different image-potential states. The spin-dependence of the lifetime within one image-potential state is rather small, e.g., the ratio between the majority and minority lifetimes of the $n=2$ state was determined to be 1.34 on 3 ML Fe/Cu(100) [*Schmidt et al.*, 2007]. Therefore, at zero pump-probe delay a change of the original spin polarization of $\Delta P = +0.1$ has to be encountered due to the spin-dependent dynamics, i.e. the preceding population and decay of the image-potential state [*Schmidt*, 2007].
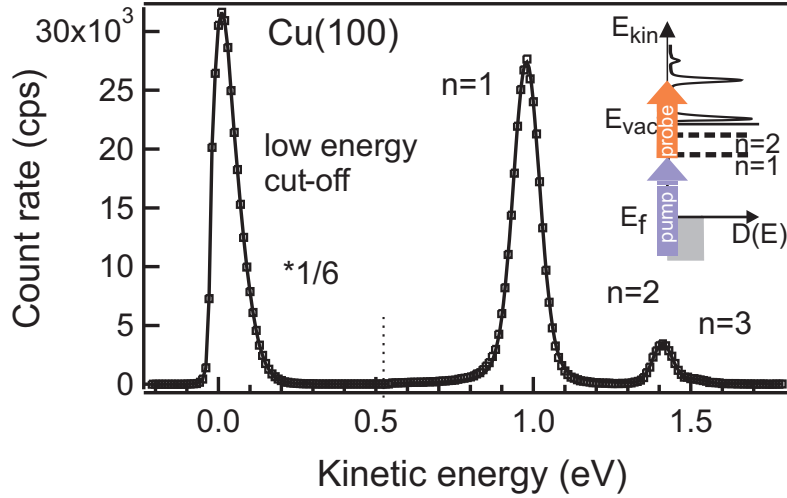
Figure 4.1: *Spin-integrated 2PPE spectrum. Data are recorded with a pump-pulse photon energy of $h\nu_{pump} = 4.67$ eV, which is larger than the sample work-function. This causes direct photoemission, visible at the low energy cut-off. The n=1 and n=2 image-potential states can be seen separately, while n≥3 image-potential states appear as a shoulder at the high-energy side of the n=2 state.*

4.1.2 Spin-resolved spectroscopy

In this section we will present data for ferromagnetic thin films. Figure 4.2 shows a spin-resolved 2PPE spectrum of a 3 ML iron film on Cu(100). Before discussing the spin-resolved spectra we have a look at the respective integrated spectrum, indicated by open square symbols (□). While the $n=1$ and $n=2$ image-potential states are clearly observable, the intensity at the low energy cut-off is almost negligible. As the work function is larger than the pump-pulse photon energy only thermally excited electrons are photoemitted by the pump pulse. The spin-integrated spectrum shows no indication for any exchange splitting of the image-potential states. As evident below, the experimental and lifetime broadening of the image-potential state is larger than the exchange splitting. However, only the spin-resolved spectra clearly reveal:

- Spin-dependent binding energies (equivalent to exchange splitting)

- Spin-dependent intensities (equivalent to spin polarization[1])

- Spin-dependent linewidths

for both, the $n=1$ and the $n=2$ state. We will show later that also the $n=3$ state and the low-energy cut-off is accessible.

---

[1]The spin-polarization is given by the asymmetry of the majority and minority count rate of the integrated peaks $P = \frac{N_{maj} - N_{min}}{N_{maj} + N_{min}}$
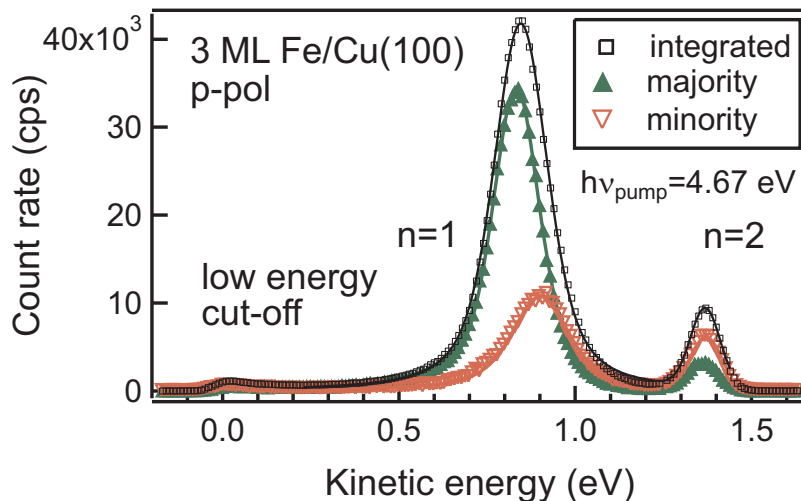
Figure 4.2: *Spin-resolved and spin-integrated 2PPE spectrum of 3 ML Fe/Cu(100). The binding energies and intensities of the image-potential states are spin dependent.*

Spin-dependent dynamics

Although we will focus on spin-dependent intensities, some comments on spin-dependent dynamics seem appropriate.

From a linewidth analysis of the n=1 state in inverse-photoemission spectroscopy [*Passek et al.*, 1995] a faster decaying minority image-potential state was deduced. Previous spin-resolved 2PPE measurements could only focus on the dynamics of excited electrons slightly above the Fermi level, the so-called hot-electrons [*Aeschlimann et al.*, 1997]. The lifetime of majority bulk electrons is about 1.5 times larger than the lifetime ofthe minority bulk electrons. These measurements did not allow to distinguish between electron-electron scattering processes between electrons with opposite or equivalent spin. Nevertheless, recent spin-resolved 2PPE data of hot-electrons on ultrathin cobalt films was interpreted in terms of magnon excitations and spin-flip processes [*Cinchetti et al.*, 2006].

Our results on spin-dependent dynamics of the image-potential-state electrons are published in [*Schmidt et al.*, 2005, 2007] and will be examined in detail by [*Schmidt*, 2007]. In brief, time-resolved measurements of the n=1,2 and n=3 states reveal a larger decay rate of the minority electrons compared to the majority electrons [*Schmidt et al.*, 2005, *Pickel et al.*, 2006]. This additionally manifests in a different linewidth for majority and minority states as a function of the pump-probe delay. The ratio of majority versus minority lifetimes is little different between iron and cobalt thin films. In contrast, intraband decay within the image-potential-state band is much stronger on iron than on cobalt. For iron the increase of the decay rate with energy above the band bottom is about twice

as large in the majority than in the minority image-potential-state bands. We interpret this in terms of magnon-enhanced exchange scattering between opposite spin bands [*Schmidt*, 2007].

4.2   Spin polarization

One of the remarkable features of the spectra in Figure 4.2 is the spin polarization of the image-potential states on 3 ML Fe/Cu(100) and in particular the difference in the spin polarization of the $n=1$ and $n=2$. Since the image-potential states are unoccupied states, the observed spin polarization must be related to the initial states probed via the excitation process.

This becomes evident, when comparing our data to previous spin-resolved inverse-photoemission experiments which always yield equal intensities of minority and majority image-potential states (see e.g. [*Passek and Donath*, 1992]). In inverse photoemission electrons decay radiatively from initial states well above the vacuum level into the image-potential states. The electrons of the initial states are provided by an electron beam, which can be spin polarized. The radiation is recorded as a function of the kinetic energy of the incoming electron beam. Since the transition matrix elements from the initial states to the image-potential states are spin independent as well as the intensity of the incoming electron beam the spin polarization of the image-potential states is zero.

Likewise for cobalt we find a pronounced spin polarization of the image-potential states. The spectrum in Figure 4.3 recorded for 6 ML Co/Cu(100) and at a photon energy of $h\nu_{pump} = 4.67$ eV reveals negative spin-polarization for both the $n=1$ and the $n=2$ image-potential states. This already suggests that the initial states probed in cobalt differ from those probed in iron.

In the following sections we will discuss the influence of the pump-pulse polarization and photon energy on the spin polarization of the image-potential states.

4.2.1   Light-polarization dependence

Spectra for ultrathin iron and cobalt films have already been presented in the previous section (see Figures 4.2 and 4.3). They were recorded using p-polarized pump and probe pulses. The corresponding spectra recorded with s-polarized pump light can be seen in Figure 4.4. Three remarkable differences are observed:
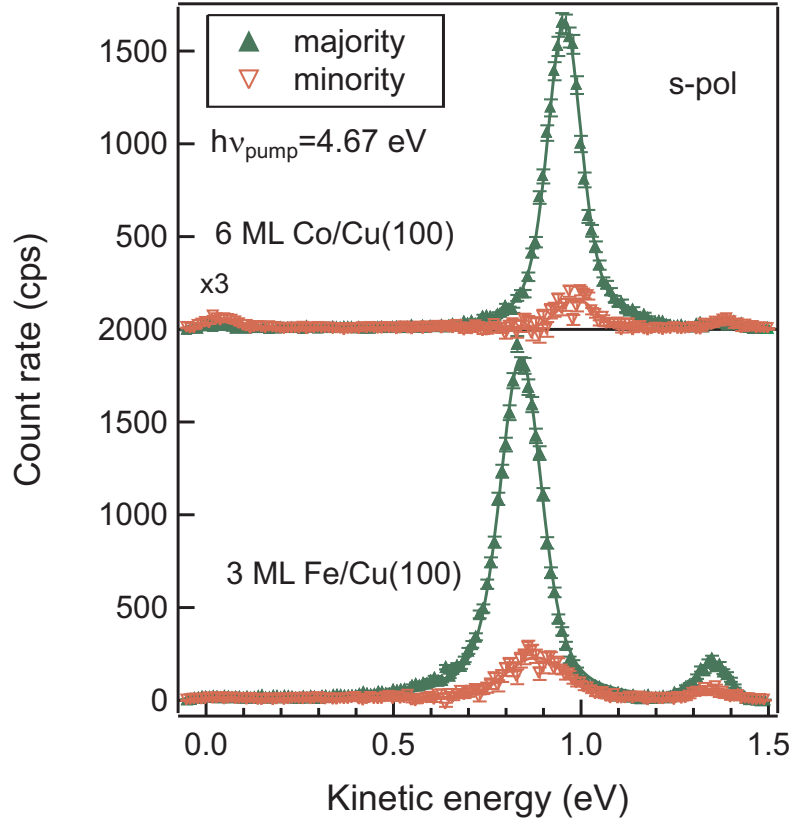
- *Different spin polarization of the image-potential states compared to the corresponding p-polarized spectra* [*Pickel et al.*, 2006]. As discussed in Section 2.3.2 the light polarization determines the initial states from which electrons are excited to the image-potential states. The dipole selection rules show that initial states excited with a p-polarized pump-pulse belong to the Δ_1 or Δ_5 representations. In contrast a s-polarized pump-pulse probes exclusively states with Δ_5 symmetry.
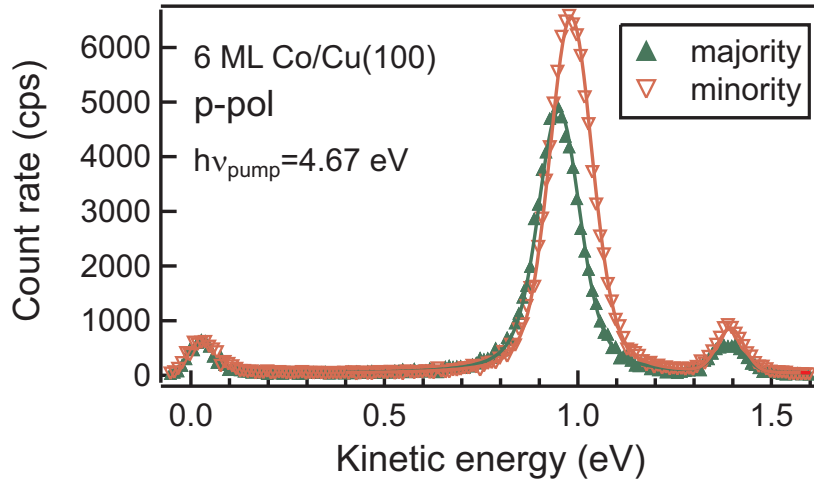
Figure 4.3: *Spin-resolved 2PPE measurements of 6 ML Co/Cu(100) measured at room temperature. The spin polarization in the n=1 state has considerably changed compared to 3 ML Fe/Cu(100) (see Figure 4.2).*

A different intensity of the $n=1$ image-potential state for excitations with s- and p-polarized light has already been observed in spin-integrated 2PPE measurements on ferromagnetic systems [*Thomann et al.*, 1999, 2000, *Wallauer and Fauster*, 1996]. The change of the spin polarization leads to different intensities of majority and minority components. This and the exchange splitting causes a shift of the center of mass between spin-integrated spectra recorded for s- or p-polarized pump pulses.

- *Different ratio of the n=1 and n=2 image-potential-state intensities compared to the p-polarized spectra.* This ratio ranges from 1.1 for the minority peak in the p-polarized measurements of 3 ML Fe/Cu(100) to about 25 for the majority peak in s-polarized measurements of 6 ML Co/Cu(100) (see Figure 4.4). Obviously, the initial-state distribution is strongly inhomogenous and depends on the ferromagnetic system and the symmetry of the states.

- *Lower count rate for measurements with s-polarized light.* This can be explained considering the overlap between the wave functions of the image-potential states and the initial states [*Wallauer and Fauster*, 1996]. Image-potential states are supported by the sp-band gap of the projected bulk band structure. Therefore, based on symmetry arguments they have a larger overlap to sp states as compared to d states. Dipole selection rules allow transitions from sp states to the image-potential states for p-polarized light whereas for s-polarized light only initial d-states with Δ_5 symmetry are excited.

Figure 4.4: *Influence of the s-polarized pump pulse on spin-resolved 2PPE spectra for 3 ML Fe/Cu(100) and 6 ML Co/Cu(100). The intensity and also the spin polarization changes compared to the corresponding p-polarized measurement in Figure 4.2 and 4.3.*

4.2.2 Pump-pulse photon-energy dependence

6 ML Co/Cu(100)

To unequivocally prove that the spin polarization of the image-potential states is determined by the initial states the photon energy of the pump pulse has to be tuned. This leads to a corresponding change of the initial states. In the following we present data from ultrathin cobalt films grown at 100 K and subsequently annealed as described in Section 3.2. The data was recorded at a temperature of 100 K. Spin-resolved 2PPE spectra for 6 ML Co/Cu(100) obtained with three different photon energies are plotted in Figure 4.5. The energy scale refers to the intermediate states, i.e. the image-potential states. As expected their binding energy is independent of the photon energy. In the spectrum recorded with a pump-pulse of $h\nu_{pump} = 4.43$ eV the photon energy is too small to excite the $n=2$ and $n=3$ states. The same holds in the the spectrum recorded with $h\nu_{pump} =$

4.68 eV for the $n=3$ image-potential state. More important, the spin polarization of the image-potential states is different for the three photon energies.
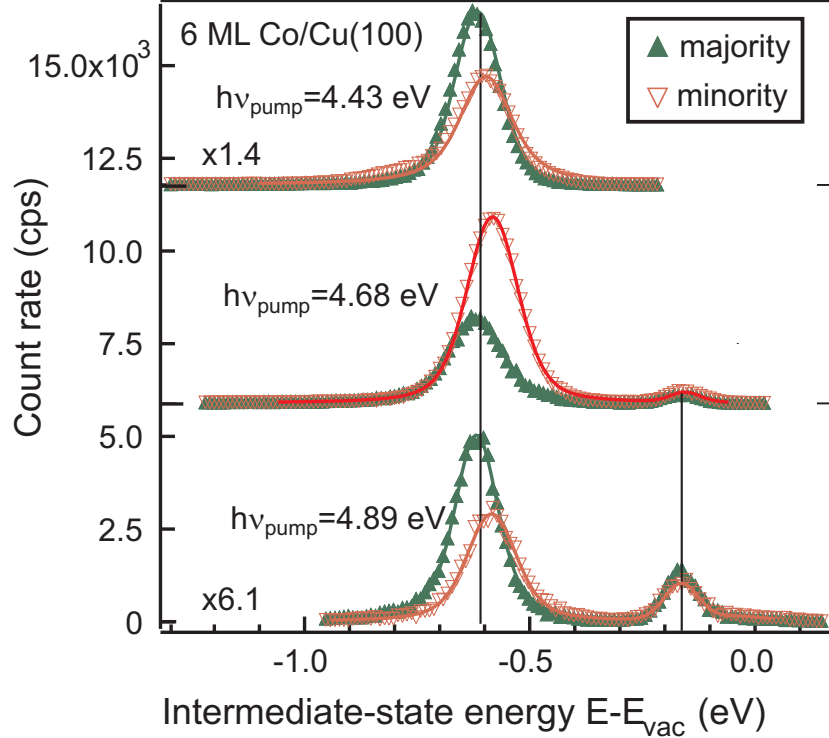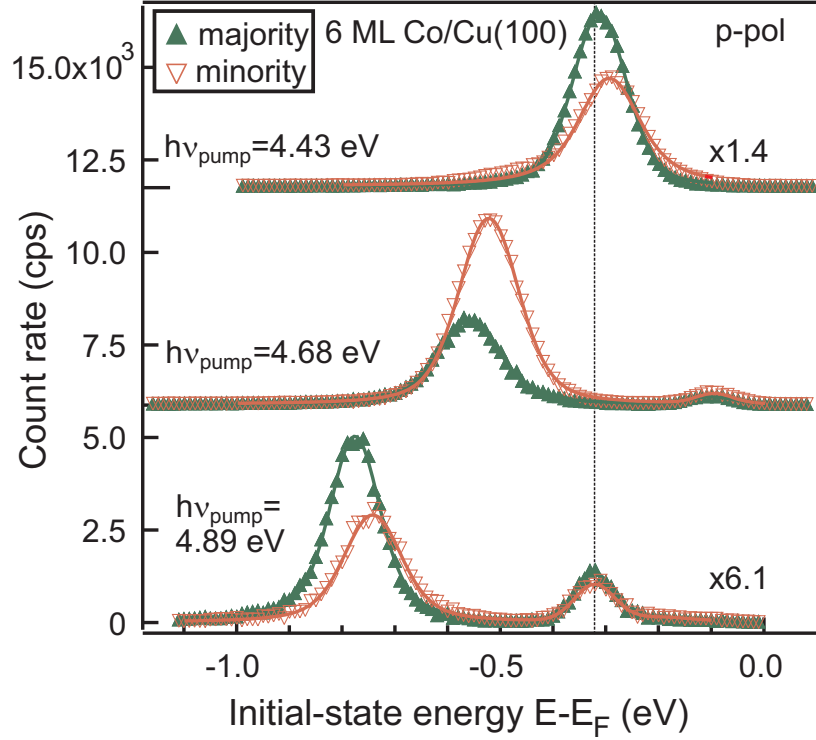

Figure 4.5: *Pump-pulse photon-energy dependence of spin-resolved 2PPE spectra of 6 ML Co/Cu(100). The spectra are plotted versus the intermediate-state energy. Therefore the peak position of the $n = 1$ and $n = 2$ state is constant. In contrast the spin polarization in the image-potential states changes significantly.*

To clarify the origin of the spin polarization, in Figure 4.6 the spectra are plotted versus the initial-state energy. As indicated by the vertical line the $n=1$ state of the spectrum with $h\nu_{pump}=$ 4.43 eV is populated from the same initial states as the $n=2$ state of the spectrum with $h\nu_{pump}=$ 4.89 eV. An equivalent spin polarization of the peaks is clearly observable [2]. This is a proof that the *spin polarization is completely determined by the initial states*. By varying the photon energy one can *sample the spin polarization of the initial states over a broad range of energy*.

Let us at first have a look on the corresponding spectra in Figure 4.7, obtained with s-polarized light. As explained above, now initial states of Δ_5 symmetry are excited. Again the spin polarization of the $n=1$ state equals that of the $n=2$

---

[2]The small deviation can be attributed to a small delay (15 fs) at which the spectrum with $h\nu_{pump} = 4.43$ eV was recorded.

Figure 4.6: *Pump-pulse photon-energy dependence of spin-resolved 2PPE. The spectra from Figure 4.5 are plotted versus the initial-state energy. The spin polarization follows the initial state energy, as can be seen by inspecting the n=1 peak of the top spectrum and the n=2 peak of the spectrum at the bottom. The line indicates their common initial-state energy.*

state for pump-pulse photon energies of 4.43 eV and 4.89 eV. This nicely proves our statement that 2PPE reflects the spin polarization of the initial-states.

We will now proceed to use the image-potential states as a sensor with respect to the spin polarization of the initial states, which is given by

$$P = \frac{N_{maj} - N_{min}}{N_{maj} + N_{min}} \tag{4.1}$$

with N refering to the area of the $n=1$, $n=2$ peak and in case of reasonable count rates also to the are of $n=3$ peak. The spin polarization of the image-potential states can be mapped versus initial state energy for measurements with different photon energies and pump-pulse polarizations. This is shown for p- and s-polarized light in Figure 4.8 for initial-state energies in between 0.8 eV and the Fermi level.

From this figure we cannot yet assign a change in spin polarization to either an enhancement or a lowering of one or the other spin channel. To sort this out, we have to consider the absolute intensities. This, however, would only be
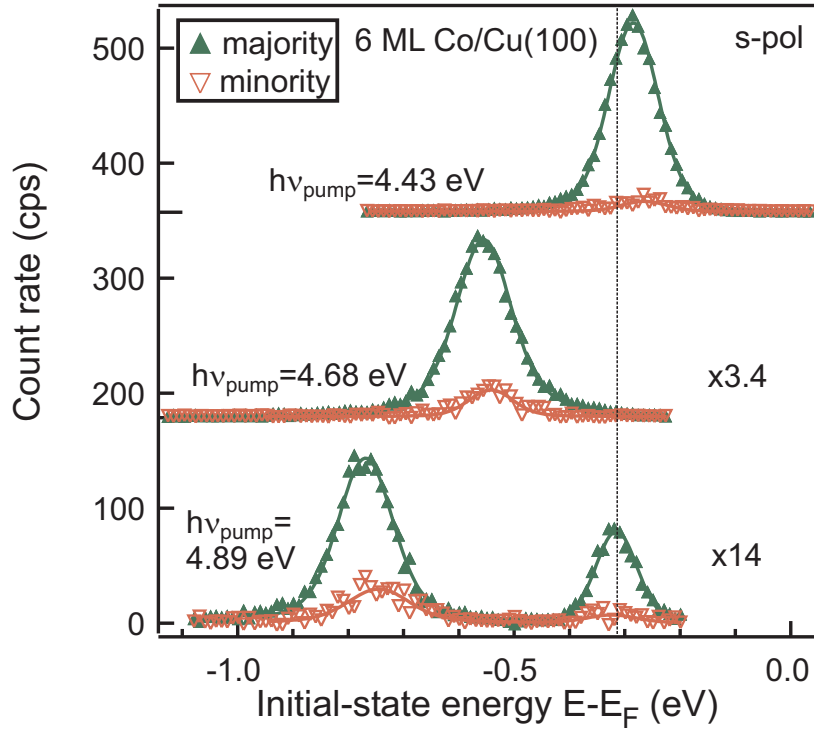
Figure 4.7: *Pump-pulse photon energy dependence of spin-resolved 2PPE on 6 ML Co/Cu(100) for s-polarized pump pulse. The spin polarization is pinned to the initial-state energy.*

possible if experimental parameters for all measurements, e.g. laser power and pulse shape, are identical, which is not fulfilled when varying the photon energy. However, we can compare the intensity of the $n=1$ and $n=2$ state within one spectrum or we can compare spectra obtained with different light polarization, but common photon energies.

The p-polarized measurements reveal a strong negative spin polarization at an initial-state energy of about $E - E_F = -0.45$ eV and a negatively spin-polarized feature at the Fermi energy. The strong negative spin polarization is due to a large minority count-rate and not due to a small majority intensity. This can be deduced from a comparison of the ratio of the $n=1$ to the $n=2$ intensity, which is much larger for the spectrum with $h\nu_{pump}$=4.68 eV than with $h\nu_{pump}$=4.89 eV. The same conclusion can be drawn by inspecting count rates of the $n = 1$ states in the p- and s-polarized measurement.

The data obtained with s-polarized light shows a high positive spin polarization, which drops off to a slightly negative value close to the Fermi level. Again the question arises whether the polarization loss is due to a reduction in majority count-rate or a rise in minority count-rate. Since the $n=2$ image-potential state has not been measured for a photon energy of 4.68 eV in Figure 4.7 we will

demonstrate this effect with the spectra for the corresponding room-temperature film of Figure 4.4. Here a very low count rate is evident in the $n=2$ state, which is populated by electrons from initial states close to the Fermi level. Therefore, we can conclude that the change in spin polarization is indeed caused by the reduction of the majority count-rate.

To summarize we could identify the following initial-state properties:

- We observe a dominant minority state with Δ_1 symmetry at about $E-E_F = -0.45$ eV

- A dominant majority state with Δ_5 symmetry exists up to $E-E_F = -0.2$ eV with a rapid drop above this energy

- From $E - E_F = -0.2$ eV up to the Fermi level we find a minority state with Δ_1 symmetry. In this case a decline in intensity of a corresponding majority state cannot be ruled out, but seems unlikely.
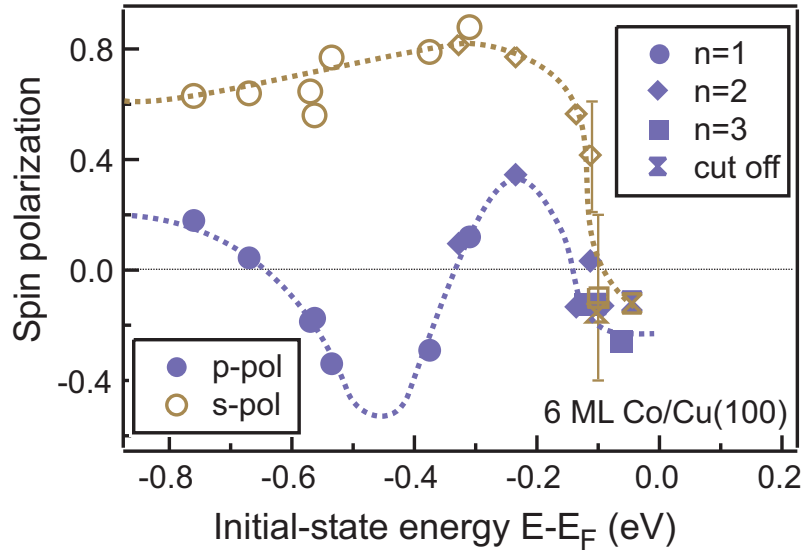
Figure 4.8: *Variation of the spin polarization of the image-potential states as a function of the initial-state energy for 6 ML Co/Cu(100). The different colors refer to the different pump-pulse polarizations, whereas the symbols denote the intermediate state or in the case of the cut-off the initial state. For comparison the spin polarization of the low energy cut-off is included. The dotted lines serve as a guide to the eye.*

To start the discussion on the above results let us have a look at the cobalt bulk band structure taken from [*Fauster*, 2006]. The possible initial and intermediate states along the Δ direction are shown in Figure 4.9. Beside the electronic band structure the transition matrix elements are of importance, which are on one hand determined by the dipole selections rules and on the other hand by the

overlap between the initial- and intermediate-state wave-functions. To explain the overlap between the image-potential states and the bulk states we follow the arguments of [*Wallauer and Fauster*, 1996, *Thomann et al.*, 1999, 2000]. They were used to derive the exchange splitting from spin-integrated 2PPE. Later on they were also adopted by [*Pickel et al.*, 2006, *Andreyev et al.*, 2006] to explain spin-resolved 2PPE spectra.

As explained in Section 2.1 the image-potential states exist only within the band gap of the projected bulk band-structure. Their wave function inside the crystal can be described by an exponentially decaying sinusoidal wave with a periodicity of π/d (see Figure 2.2), where d is the *out-of-plane* lattice constant [*Fauster*, 1994]. In other words, the periodicity of the image-potential states is given by the k-vector at the Brillouin zone boundary, the X-point for an fcc crystal. Therefore, the overlap with initial states having a wave vector close to the X point is large and excitations from these states will dominate the 2PPE signal. This is indicated in Figure 4.9 by the thickness of the vertical arrows, which qualitatively resembles the excitation probability.

Firstly, we concentrate on the excitation process with s-polarized light (see right panel in Figure 4.9). For initial states up to binding energies slightly below the Fermi level excitations from the Δ_5 majority band should dominate since these states are closer to the X-point than their minority counterpart. However, only the minority band crosses the Fermi level, which should lead to a negative spin polarization at the Fermi energy. Such a decline in spin polarization is indeed observed as discussed above and shown in Figure 4.8. The excitation scheme indicated by the arrows in Figure 4.9 corresponds to a photon energy of 4.68 eV (cf. Figures 4.2 and 4.4). Especially in Figure 4.4 a decline of the 2PPE intensity close to the Fermi level manifests by the very low count rate of the $n=2$ state. Here it becomes evident that the complete majority Δ_5 band is located below the Fermi level. This suggests fcc Co being a strong ferromagnet, i.e. no majority d states exist at the Fermi level. We note that these measurements do not provide an unique proof, since only d states with Δ_5 symmetry contribute to the spectrum. However, the Δ_2 band, which is omitted from the band structure in Figure 4.9, crosses the X point below the Δ_5 band [*Schneider et al.*, 1991a]. One may argue that only states along the Δ direction have been measured. However, band-structure calculations for Co(100) in [*Andreyev et al.*, 2006] indicate that the energy of the d bands has its maximum in this direction.

In this publication also spin-resolved 2PPE and spin-resolved 1PPE spectra of 2-20 nm thick cobalt films on Cu(100) were presented. At an energy of $E - E_F = -0.4$ eV a state with majority spin polarization was observed and attributed to a d state. This is consistent to our data except for a slight energy offset. In this experiment the excitation process was not via the image-potential states due to a smaller pump-pulse photon energy compared to the photon energy used in our experiment. An image-potential resonance could only be observed, when reducing the work function by Cs-doping.

In case of p-polarized light transitions from initial states with Δ_1 and Δ_5 symmetry are allowed. However, the latter states have been neglected due to the dominant overlap between image-potential states and the *sp* states of Δ_1 symmetry. As already discussed, the spin polarization of spectra obtained with p-polarized light shows two features. The first can be ascribed to a minority state at -0.45 eV . One possible candidate could be the minority band-bottom of the Δ_1 band at about -1 eV in spite off the large offset of 0.55 eV (see Figure 4.9). The second feature, the negative spin polarization at the Fermi level may only be assigned to the flat Δ_1 band at the Γ point. However, as explained above the excitation probability from this point with $k=0$ should be very small.
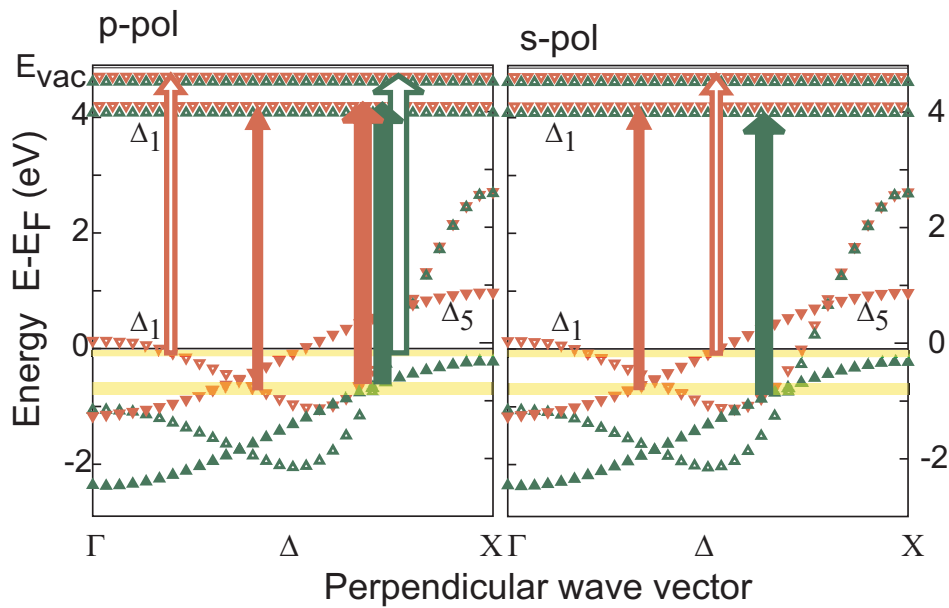
Figure 4.9: *Excitation process in spin-resolved 2PPE for fcc Co in a simple model employing a non-relativistic bulk band-structure (after [Wallauer and Fauster, 1996]). States have been omitted which do not contribute to the signal due to the dipole selection rules. Open triangles refer to Δ_1 type states, solid triangles to states with Δ_5 symmetry. The arrows indicate possible excitations of the $n=1$ state (solid arrows) and of the $n=2$ state (open arrows). The colors (green for majority and red for minority) account for spin-dependent excitation, the thickness for the strength. The possible excitations with p- and s-polarized light are shown separately in the left and right panel. For p-polarized light the $\vec{A}_{\parallel}$ component of the pump pulse has been omitted.*

It is obvious that the evolution of the spin polarization can only be described to a certain degree by simply considering the bulk band-structure. Already in Section 2.1 the small overlap of image-potential states with bulk states was pointed out. The probability amplitude of the image-potential-states decays into the crystal by about a factor of two for a distance of 1.8 Å, the thickness of one monolayer

[*Thomann*, 1999]. Therefore, image-potential states are extremely surface sensitive. A large overlap between the wave functions of image-potential states and bulk states would also contradict the high spin polarization, as it can be observed for 3 ML Fe/Cu(100) (Figure 4.2). Otherwise a significant contribution from unpolarized electrons from the copper substrate should be observable. This indicates that surface resonances will contribute significantly to the signal.

To study the influence of surface resonances annealing experiments have been performed. The cobalt film was initially deposited at 100 K and then annealed to different temperatures for about 5 minutes. Between each annealing step a measurement was performed at 100 K. The resulting spectra are shown in Figure 4.10. Generally, with increasing annealing temperature a rise of the image-potential-state related peaks and a decrease in linewidth can be observed and attributed to a smoothing of the surface. Additionally, time-resolved measurements revealed an increase in lifetime. Since no significant change is observed in spin polarization and exchange splitting for an annealing-temperature range from room temperature up to 490 K we exclude any significant alloying or Cu segregation, which was observed in STM measurements already at 450 K [*Schmid et al.*, 1993]. One should also note the similarity between room-temperature grown and annealed films (cf. Figure 4.1 and 4.6).

With respect to the spin polarization the following conclusions can be drawn. The spin polarization is positive at $E - E_F = -0.35$ eV for the non-annealed sample. Starting at an annealing temperatures of 295 K the spin polarization becomes negative. Simultaneously, image-potential states appear at this annealing temperature. This strongly suggests, that the feature is closely related to a smooth surface.

Recently, a $3d$ surface resonance was found at 6.5 ML Co/Cu(100) by spin- and angle-resolved photoelectron spectroscopy at $E - E_F = -0.36$ eV [*Miyamoto et al.*, 2006]. In the same experiment also an initial state with negative spin-polarization is observed at about $E - E_F = $ -0.12 eV, which could not be related to a surface resonance. Both states and their spin polarization are consistent with our findings. They are furthermore corroborated by calculations of photoemission spectra in normal emission for fcc Co/Cu(100) [*Braun*, 2007]. Density functional theory reveals a negatively spin-polarized surface resonance at $E - E_F = $ -0.6 eV.

From literature no other evidence for a minority surface resonance with Δ_1 symmetry is found. Most experiments performed on Co/Cu(100) focused on the Δ_5 band, and its exchange splitting [*Clemens et al.*, 1992b,a]. *Schneider et al.* [1991a] used spin-resolved photoemission to map the band structure and compered it with band-structure calculations. In general, the experimental results are consistent with the measurements we performed with s-polarized light, especially the strong reduction of the majority count-rate at the Fermi level. We postpone a further discussion until Section 4.3.6, where the dependence of the electronic structure on the film thickness as well as relativistic effects will be included.
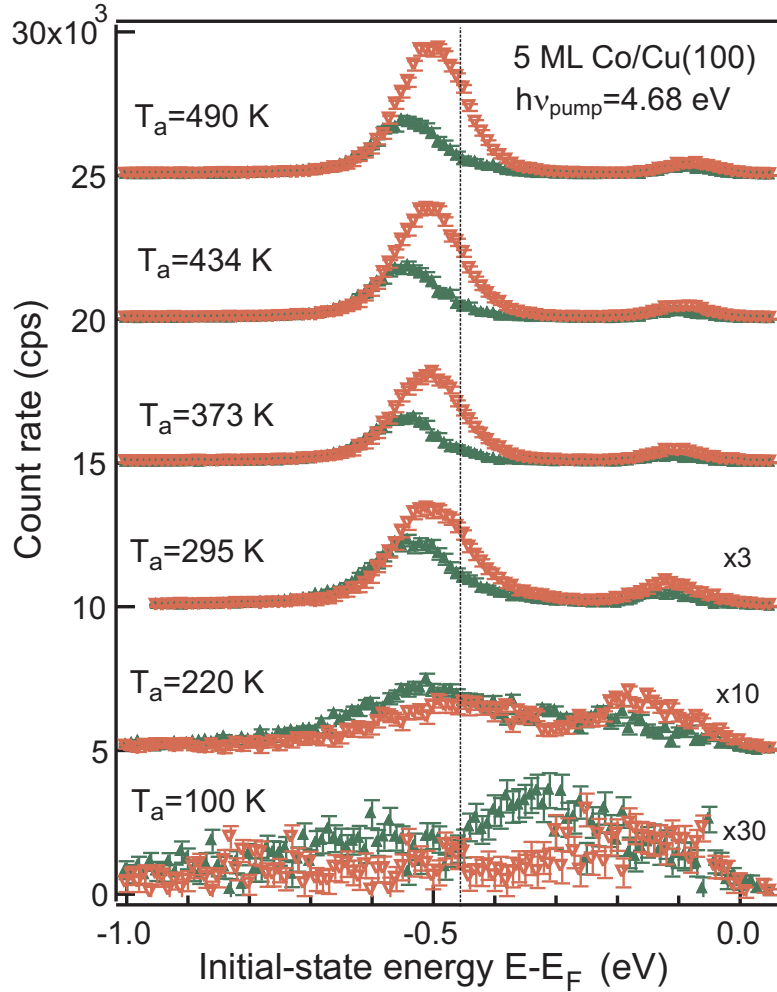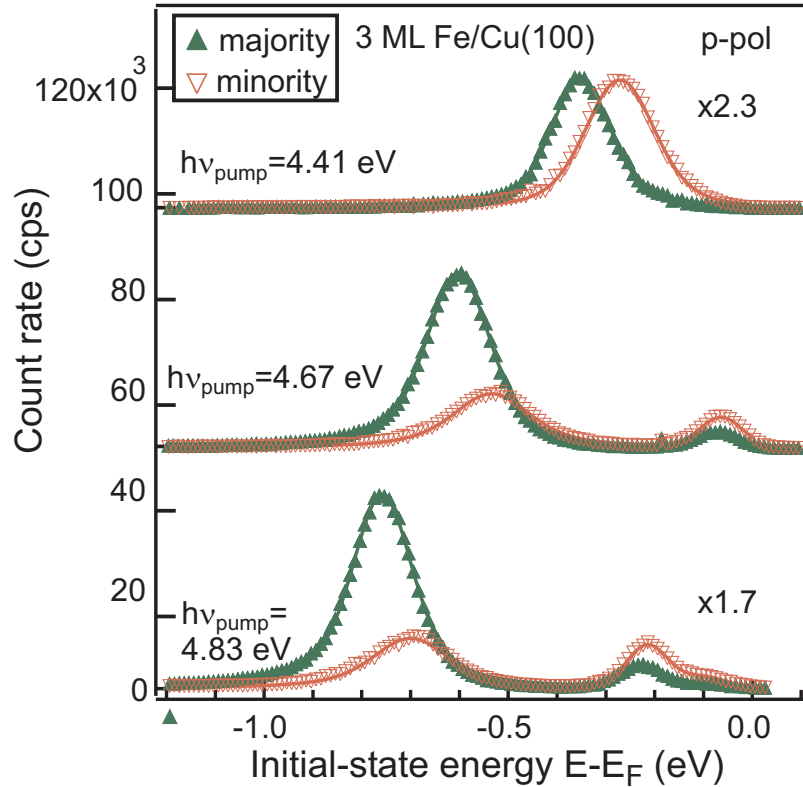
Figure 4.10: *Dependence of spin-resolved 2PPE spectra of 5 ML Co/Cu(100) on the annealing temperature. The image-potential states as well as the negative spin polarization at $E - E_F$= -0.45 eV becomes visible at annealing temperatures of about 200 K - 295 K.*

3 ML Fe/Cu(100)

Measurements similar to those for 6 ML Co/Cu(100) have been performed for 3 ML Fe/Cu(100) grown at room temperature. The spectra are plotted in Figures 4.11 and 4.12 as a function of the initial-state energy for p- and s-polarized pump pulses. In analogy to Co/Cu(100) we now evaluate the spin polarization for each peak. The resulting spin polarization for p- and s-polarized light is shown in Figure 4.13 as a function of initial-state energy. With s-polarized light an almost constant positive spin polarization is observed. The p-polarized spectra reveal a strong change of the spin polarization, starting from $P=+0.5$ at an energy of $E - E_F = -0.7$ eV and decreasing to $P=-0.4$ at -0.2 eV. This strong decrease is

attributed to a change of the minority count-rate, which becomes obvious when inspecting the ratio of the amplitudes between the $n=1$ and $n=2$ minority states in Figure 4.11. The value is about 1:1 and therefore a significant enhancement of minority states close to the Fermi level can be deduced, while at at an energy of $E - E_F = -0.6$ eV a reduction of minority electrons is obvious.
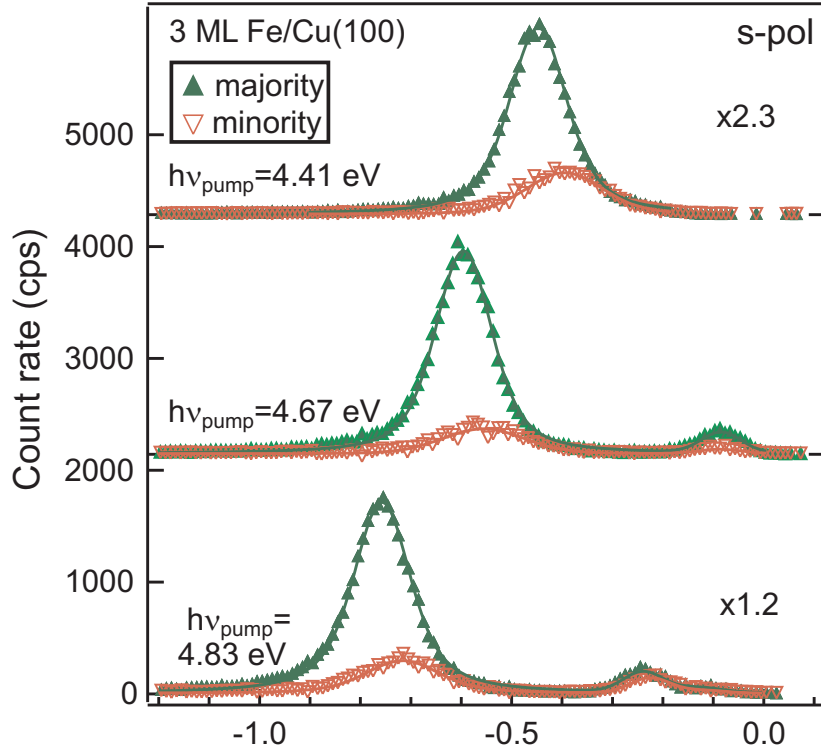

Figure 4.11: *Pump-pulse-photon-energy dependence of spin-resolved 2PPE spectra for 3 ML Fe/Cu(100).*

We again consider an fcc bulk band structure including the possible excitations shown in Figure 4.14. The band dispersion for iron and cobalt is identical but the iron band-structure has been shifted by $+0.4$ eV to account for the change in d-band occupancy. For s-polarized light ($\vec{A}_{\|}$) we mainly probe the Δ_5 majority-band and therefore observe a nearly constant positive spin polarization over the accessible energy range. What is more, the data also confirms the positive spin polarization at the Fermi level. This demonstrates that the majority d band is crossing the Fermi-level, and therefore that 3 ML Fe/Cu(100) are a weak ferromagnet.

The excitation process with p-polarized light (dominantly $\vec{A}_\perp$) is expected to yield strong positive spin polarization when initial states are probed which are below the band bottom of the minority band at $E - E_F = -0.6$ eV. Above,

Figure 4.12: *Pump-pulse-photon-energy dependence of spin-resolved 2PPE spectra for 3 ML Fe/Cu(100) as in Figure 4.11 but with s-polarized pump-light.*

there should be a strong rise in the minority channel, which can even lead to a negative spin polarization, due to the rather broad minimum of the minority Δ_1 band. At the Fermi level the majority and minority bands have almost the same k-vector and equal dispersion. If we consider a small contribution from the minority electrons from the Δ_1 band close to the Γ-point, we still expect a negative spin polarization. In our data we observe a decrease in spin polarization starting at an energy of about $E - E_F = $ -0.5 eV. The minimum is reached at about $E - E_F = $ -0.1 eV. Since we have to consider the spectral width of the pump pulse and dephasing between the initial and intermediate state, we don't expect the minimum of the spin polarization in our measurements at the energy of the band minimum. $E - E_F = $ -0.25 $\pm$0.15 eV might be a good estimate which is shifted by 0.35 eV as compared to the value taken from the bulk band-structure.

In general a discussion about the electronic structure of fcc iron is accompanied by the question in which ferromagnetic phase the iron exists. Total energy calculations as a function of atomic volume [*Moruzzi et al.*, 1986] predict two possible metastable configurations, a high-spin and a low-spin phase, which differ by their magnetic moment ($2.8\mu_b$ and $1.4\mu_b$). Although *Mankey et al.* [1993] interpreted data consistent to a low-spin configuration, other experimental spin-
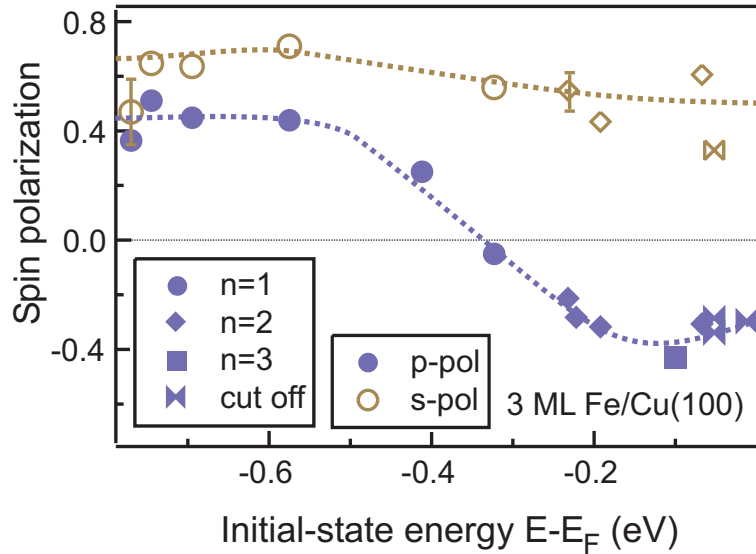
Figure 4.13: *Spin polarization of the image-potential states as a function of the initial-state energy for 3 ML Fe/Cu(100). The colors denote the different pump-pulse polarization and thus the different symmetry of the initial states. The symbols reflect the spectral feature, from which the spin polarization has been extracted. The dotted lines are guides to the eye.*

resolved photoelectron spectroscopy studies used a high-spin phase to describe their measurements [*Zharnikov et al.*, 1997, *Kläsges et al.*, 1998]. The difference in the band structure between low and high spin phase can be seen in calculations from [*Podgórny*, 1989, *Zhou et al.*, 1997]. Our results combined with the simple bulk model for initial states favor the low-spin phase, since in a high-spin phase the band bottom of the Δ_1 band should be considerably shifted upwards above the Fermi level. In this case also for excitations with p-polarized light the minority count rate should be strongly reduced.

As described above the band structure of Co was just obtained by shifting the band structure of Fe by 0.4 eV [*Thomann*, 1999]. Our data is in accordance with this assumption since the spin polarization of Co and of ultrathin Fe in Figure 4.8 and 4.13 roughly reflects this shift. The negative spin polarization obtained for iron with a p-polarized pump pulse (see Figure 4.13) may therefore also be attributed to a surface resonance with Δ_1 symmetry. The somehow broader width of the spin polarized feature in Fe/Cu(100) could be due to a lower surface quality of the iron film. Moreover, stronger non-resonant excitation of the image-potential states in Fe/Cu(100) exists due to larger dephasing, especially in the $n=1$ state [*Schmidt et al.*, 2005], which leads to a general broadening of the spin polarization.

We note that for a more elaborate interpretation surface electronic states and calculated transition-matrix elements should be used, which explicitly consider
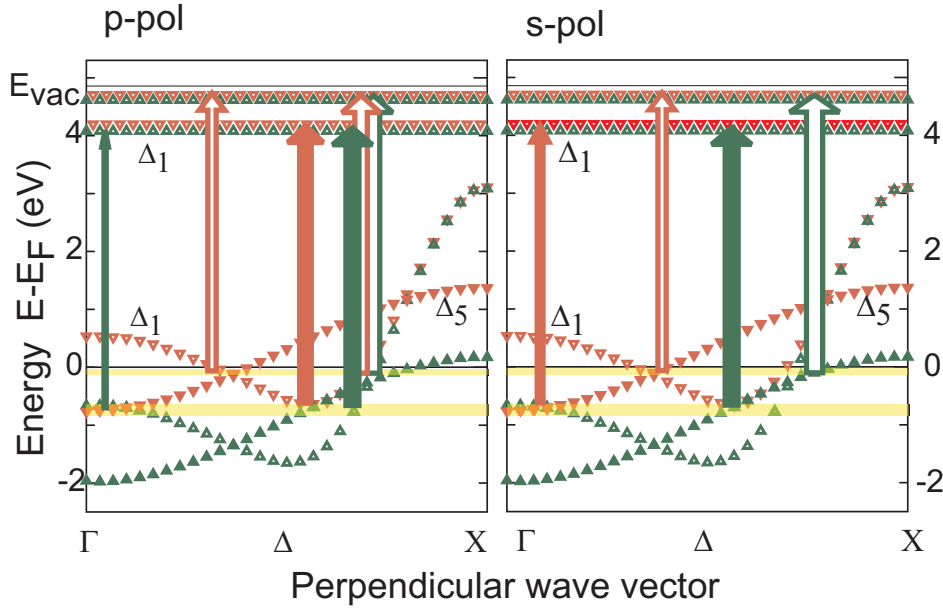
Figure 4.14: *Description of the excitations in a non-relativistic band structure of fcc Fe along the Δ direction after [*Thomann et al., *1999]. The arrows indicate possible transitions into the image-potential states (solid arrows for transitions to the n=1 state, open arrows for transitions to the n=2 state). Their color denote the spin of the excited electrons, whereas their thickness indicates the strength. The left panel shows excitation with p-polarized light (neglecting the $\vec{A}_{\parallel}$ component), the right panel with s-polarized light.*

the surface or bulk character of the initial states. With respect to the spin polarization, agreement is found with spin-polarized metastable deexcitation spectroscopy (SPMDS), a technique, which is highly surface sensitive. Here, also a negative spin polarization at the Fermi level was measured [*Kurahashi et al.,* 2003a]. Band structure calculations predict a negative spin polarization of the density of states at the surface layer [*Fernando and Cooper*, 1988]. An explicit comparison of the density of states with our results cannot be made due to the unknown transition-matrix elements.

4.2.3 Low energy cut-off

An additional spectral feature, which has been neglected in the discussion, is the low energy cut-off, which is shown for cobalt and iron in Figure 4.15. As explained above it stems from electrons directly excited by the pump pulse and is therefore only clearly resolved for photon energies which are larger than the sample work-function. The low-energy cut-off shows a spin polarization which depends on the polarization of the light pulse. Both, the spin polarization and the

intensity are almost equivalent to the values obtained from the image-potential states (cf. Figure 4.8 and 4.13).
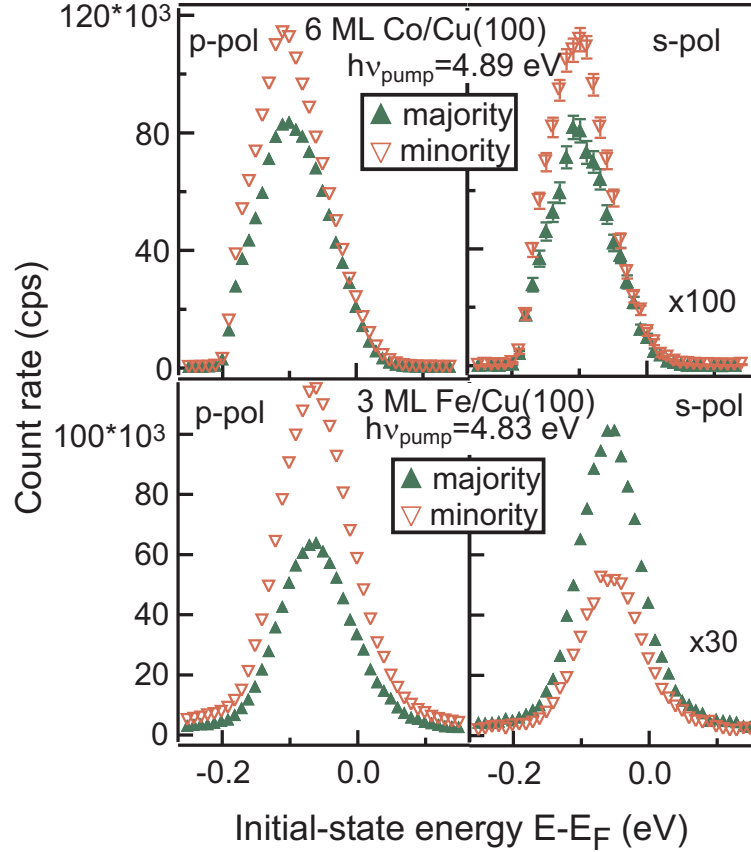
Figure 4.15: *Spin-resolved measurements of the low-energy cut-off of 6 ML Co/Cu(100) and 3 ML Fe/Cu(100) recorded with a p-polarized (left panel) and s-polarized (right panel) pump pulses. For 3 ML Fe/Cu(100) spectra have been recorded with open analyzer slits leading to a reduced energy resolution. The corresponding spin polarizations are included in Figures 4.8 and 4.13*

A connection between 2PPE via the image-potential states and direct photoemission, which contributes to the signal in the low energy cut-off seems likely. This can be understood considering the excitation process. As explained above the electrons are excited directly by the pump pulse to states slightly above the vacuum level. Around the vacuum level there are no bulk states in the projected bulk band structure, otherwise the image-potential states would become surface resonances. Therefore the final state must be a free electron wave function, whose overlap to the bulk states is only given by the exponential decaying part of the wave function into the bulk, a so-called evanescent state. This results in a strongly enhanced surface sensitivity as it is the case for the excitation via the image-potential states. Similar arguments have also been put forward by [*Bisio*

et al., 2006]. A different spectral distribution for different orders of multiphoton excitations was explained by the final state energy being either within the gap or outside.

4.3   Dichroism

4.3.1   General observation

Up to now we have presented spin-resolved spectra and studied the spin polarization with respect to the initial-state energy. In the following section, we will focus on spin-integrated measurements of ultrathin cobalt films and distinguish between spectra obtained for the two different magnetization directions. In Figure 4.16 two spin-integrated spectra of 5 ML Co/Cu(100) are shown. They were both recorded with a p-polarized pump pulse but for antiparallel magnetization directions. A remarkable difference in the count rates between the two spectra is observable, for the $n=1$ and also for the $n=2$ image-potential state. So far an experimental artifact like a laser intensity variation cannot be ruled out, but seems unlikely, due to the energy dependence of this effect. Note that the intensity difference changes sign between the $n=1$ and $n=2$ state. Measurements obtained with s-polarized pump pulses (see Figure 4.17), however, show no difference in intensity. What is more, spin-integrated time-resolved measurements reveal even a time dependence of this difference in intensity, as shown in Figure 4.18. Here, the spin-integrated spectrum of the measurement with a magnetization vector pointing upwards, as defined in the inset in Figure 4.16, shows a faster decay compared to the spectrum recorded with opposite magnetization direction.

In general, a dependence of the photocurrent on the direction of the sample magnetization is known as magnetic dichroism, in the case of linearly polarized light also as magnetic linear dichroism. It was predicted in photoemission spectroscopy over a decade ago [*Tamura and Feder*, 1991] and later on observed in various photoelectron spectroscopy studies (see e.g. [*Kuch and Schneider*, 2000]).

4.3.2   Magnetic linear dichroism explained by symmetry considerations

Following the review given by [*Kuch and Schneider*, 2000] we will start with a brief qualitative explanation for magnetic linear dichroism based on symmetry arguments. The symmetry of the experiment can be used to predict the presence of dichroism. Beside the geometric structure of the sample, the symmetry of the set-up is also determined by the photoelectron momentum $\vec{k}$, the electric field of the light $\vec{E}$ and the magnetization $\vec{M}$.
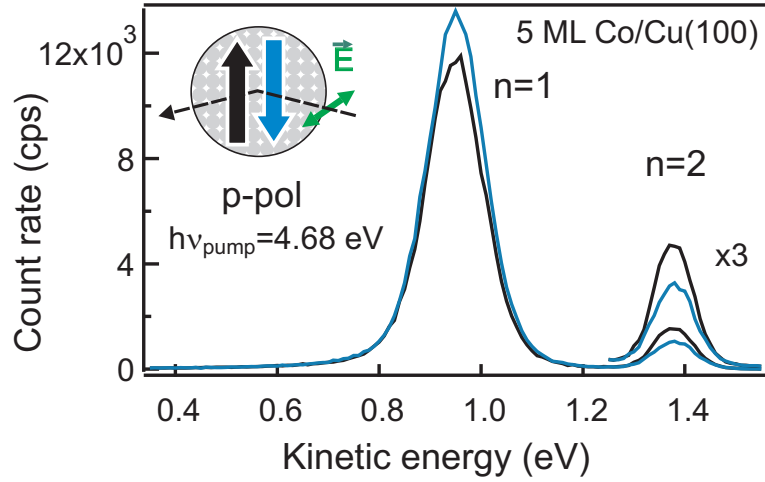
Figure 4.16: *Spin-integrated intensity dependence on the magnetization direction for 2PPE measurements of 5 ML Co/Cu(100) with p-polarized light.*
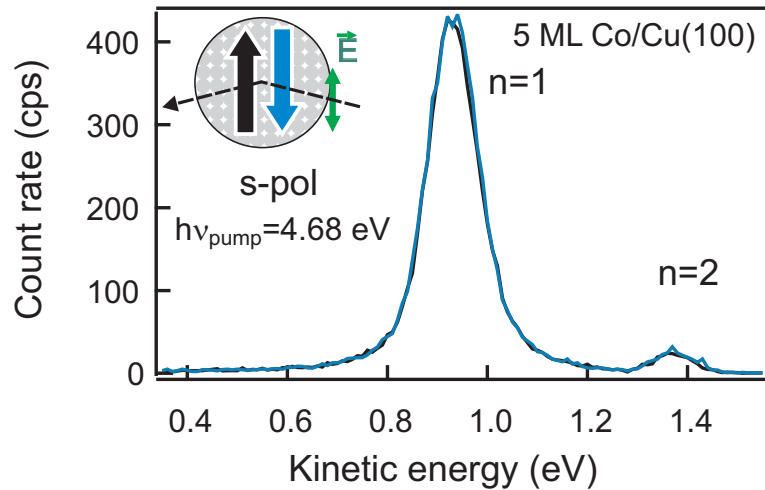
Figure 4.17: *Spin-integrated 2PPE measurements of 5 ML Co/Cu(100) for s-polarized light. No dependence of the magnetization direction on the intensity is observable.*

In terms of a symmetry based definition, dichroism exists if a transformation from $+\vec{M}$ to $-\vec{M}$ cannot be obtained by any symmetry operation which leaves the $\vec{E}$-field vector of the light and the crystal structure unchanged. Since we measure in normal emission the wave vector $\vec{k}$ lies along the main symmetry axis and is always conserved under symmetry transformations. The (100) surface of an fcc crystal restricts the symmetry operations according to C_{4v} in Schönfließ notation. The magnetization axis reduces the symmetry to C_{2v}, which includes four symmetry operations: the identity element, a reflection at the y-z plane,
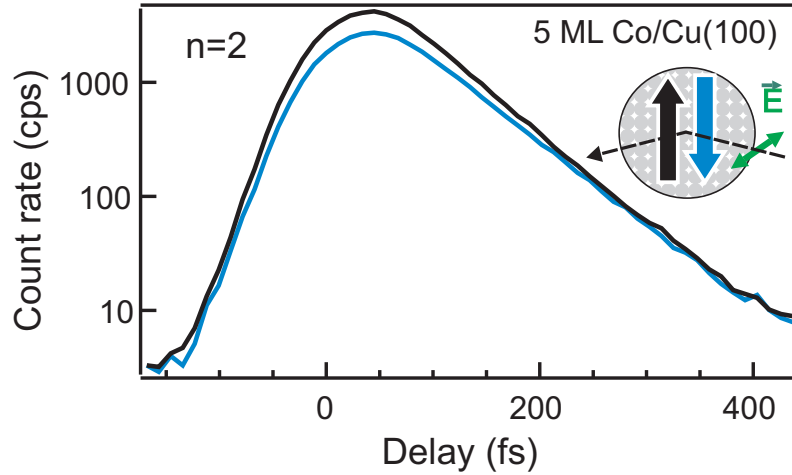
Figure 4.18: *Dependence of the spin-integrated lifetime on the magnetization direction. This is shown for the n=2 state of 5 ML Co/Cu(100).*

a reflection at the x-z plane and a rotation of π around the surface normal (z-axis). These operations, including our measurement geometry with either p- or s- polarized light, are visualized in Figure 4.19. As it can be seen in panels a) -c) neither the rotation nor any of the reflection operations can change the magnetization from $\vec{M}$ to $-\vec{M}$ without changing the $\vec{E}$-field vector for p-polarized light. However, in the case of s-polarized light (see panel d)) a reflection at the y-z plane transforms $\vec{M}$ into $-\vec{M}$ but doesn't affect the direction of $\vec{E}$ [3]. This explains the appearance of dichroism in p-polarized and also its absence in s-polarized measurements. By these symmetry considerations it should be obvious that in the case of ultrathin iron films on copper no dichroism is present, due to the *out-of-plane* magnetization, which is also in accordance with our findings.

4.3.3 Initial-state effect

We will have a look on photon-energy-dependent measurements to study the origin of the dichroism as it was also done for the spin polarization (see Section 4.2.2). In Figure 4.20 four different spectra of a 7 ML Co/Cu(100) film, obtained at different photon energies, are plotted versus the initial-state energy. To visualize the dichroism over the whole energy range, especially for the $n=2$ and $n=3$ image-potential state, the intensity is plotted on a logarithmic scale. As indicated by the dashed lines the dichroic features are pinned to the initial-state energy. This alone is a proof of an initial-state effect of the dichroic features. It becomes even more evident by quantifying the dichroism with the asymmetry A, defined by

---

[3]When performing symmetry operations one should keep in mind that $\vec{M}$ is an axial vector.
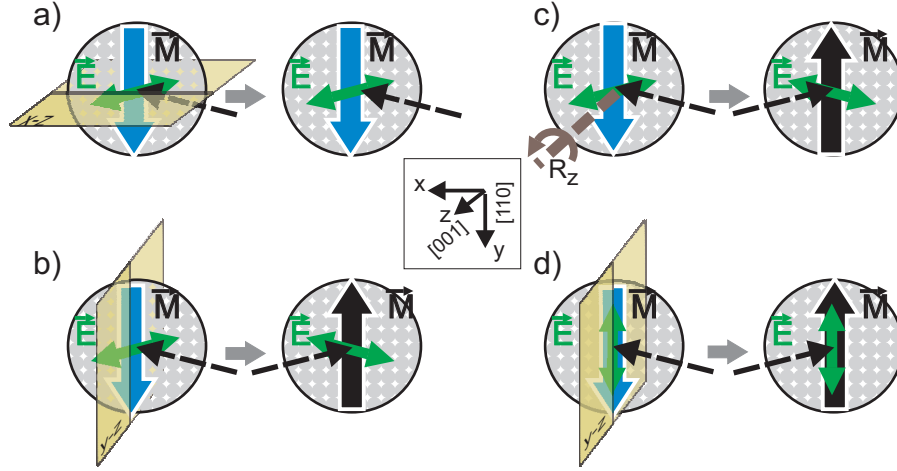
Figure 4.19: *Explanation of magnetic linear dichroism with symmetry operations on the measurement geometry. Explicitly the magnetization direction $\vec{M}$, the electric field vector of the pump light $\vec{E}$ and the crystal structure is included. a) Reflection at the x-z plane does not lead to any change of the external parameters. b) Reflection at the y-z plane changes $\vec{M}$ but also $\vec{E}$. c) A rotation of π around the normal also change both, $\vec{M}$ and $\vec{E}$. d) For s-polarized light a reflection at the y-z plane leads to a change of $\vec{M}$ but not of $\vec{E}$.*

$$A = \frac{I_\downarrow - I_\uparrow}{I_\downarrow + I_\uparrow} \tag{4.2}$$

where $I_\downarrow$ and $I_\uparrow$ denote the count rate for the magnetization pointing downwards or upwards in our set-up (see insets in the following figures). In Figure 4.21 the asymmetry is plotted versus the energy of the initial states. Here, strong dichroism is observed at energies of $E - E_F =$ -0.45 eV, -0.18 eV and -0.05 eV as well as a region with faint dichroism at $E - E_F =$ -0.7 eV, which will, however, be neglected in the following discussions. The absence of dichroism at $E - E_F =$ -0.18 eV in the spectrum with $h\nu_{pump} = 4.65$ eV and at $E - E_F =$ -0.05 eV in the spectrum obtained with $h\nu_{pump} = 4.43$ eV are likely to be explained by missing intermediate states in the respective excitation process.

Up to now we have considered spin-integrated measurements and have not made use of the spin-polarization-sensitive detection. In Figure 4.22 the corresponding spin-resolved spectra are now plotted separately for both magnetization directions. As described in the Appendix A.3 it is not straightforward to extract the spin polarization accurately from the raw data in the presence of dichroism. This might lead to a systematic error in the majority and minority count rate. Nevertheless, by comparing the spin-resolved data for the two magnetization directions it becomes obvious that *mainly the minority electron count rate changes*
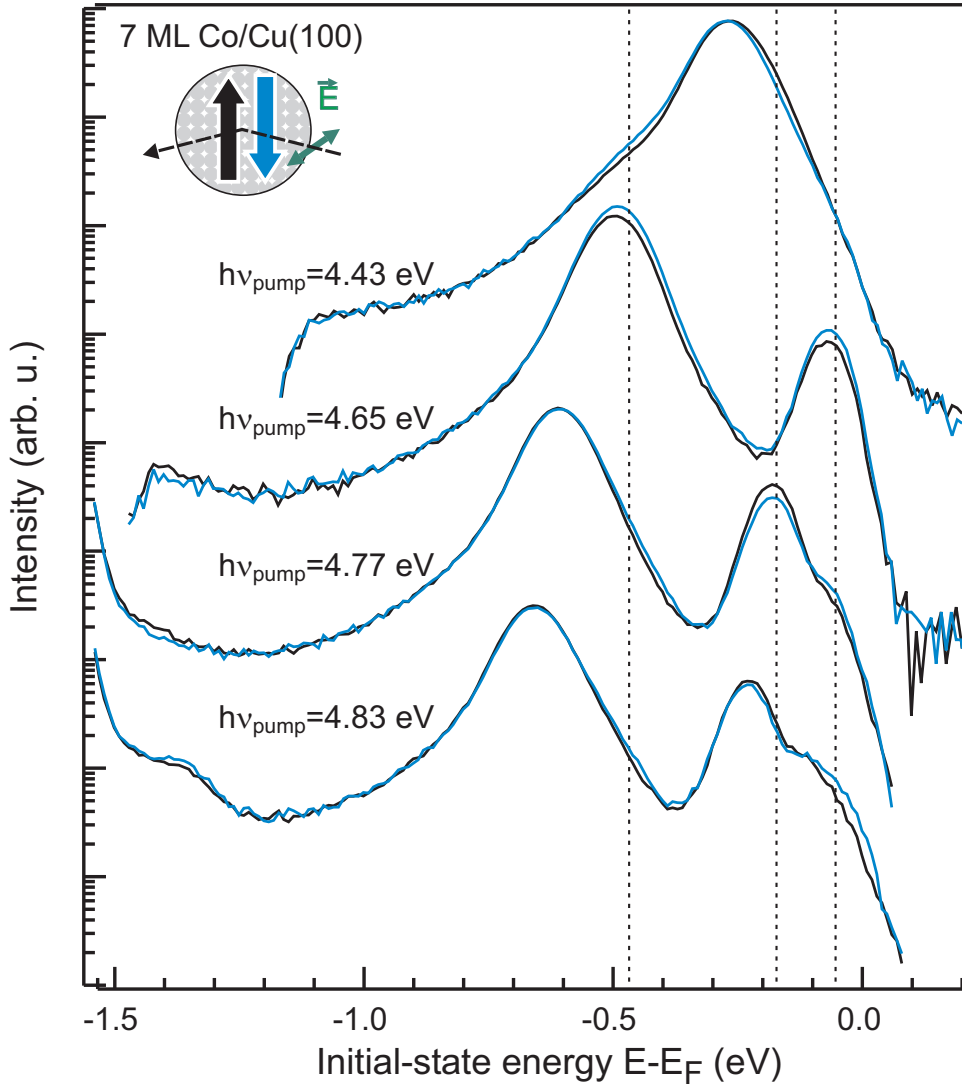
Figure 4.20: *Initial-state effect of dichroism. Spin-integrated measurements of 7 ML Co/Cu(100), which were taken at various photon energies, are plotted versus the initial-state energy. The dashed lines indicate the strong dichroism which is fixed to the initial-state energies.*

with respect to the magnetization direction. For all three dichroic features in the spectrum we may therefore speak of a minority electron effect.

An additional proof of the minority character is given by spin-integrated time resolved measurements. In Figure 4.23 three time-resolved measurements are shown, two of the $n=2$ state at two different pump-photon energies and one for image-potential states with $n \geq 3$. Due to the coherent excitation of several states the latter shows quantum beats, which have already been well studied for spin-integrated measurements [*Höfer et al.*, 1997, *Reuß et al.*, 1999] and will be
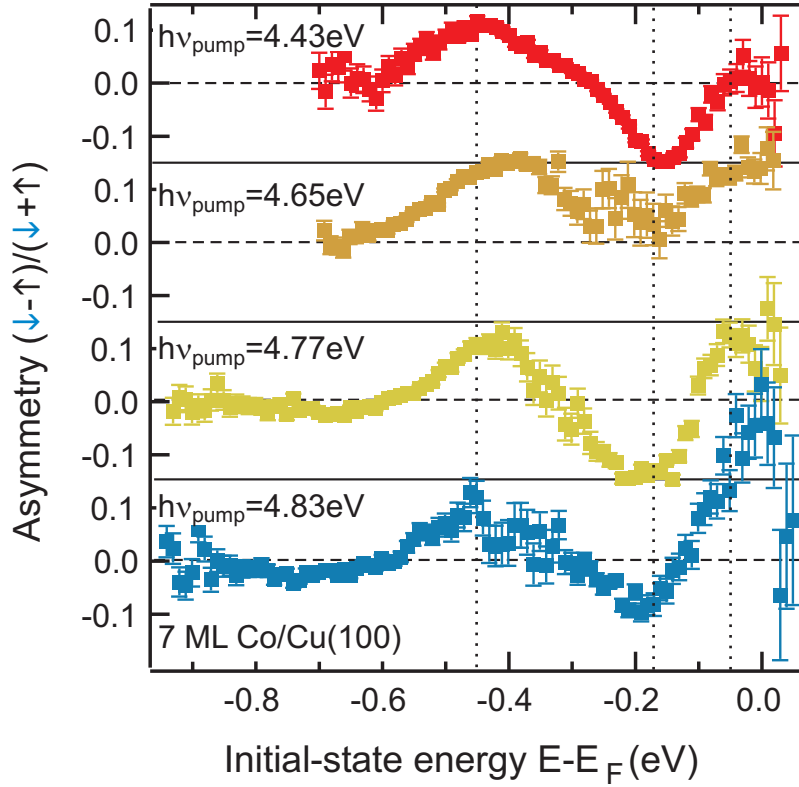
Figure 4.21: *Asymmetry of measurements from Figure 4.20 defined by $(I_\downarrow - I\uparrow)/(I_\downarrow - I_\uparrow)$. The asymmetry is fixed to the initial-state energy.*

discussed by [*Schmidt*, 2007] for spin-resolved measurements. The fact that the spin-integrated measurements have a 'dichroic' lifetime has already been taken as a proof for dichroism. Furthermore, it can be seen that the difference of the 'dichroic' lifetime of the $n=2$ image-potential state changes its sign between the two photon energies, i.e. $\tau_\uparrow > \tau_\downarrow$ @ $h\nu_{pump} = 4.65$ eV and $\tau_\uparrow < \tau_\downarrow$ @ $h\nu_{pump} = 4.77$ eV . This substantiates that the dichroism is definitely not caused by the image-potential states. The most striking feature, however, is that all dichroic time-resolved measurements *converge*. To explain this we have to recall one important fact: *Minority image-potential-state electrons live shorter than majority image-potential-state electrons* [*Schmidt et al.*, 2005, 2007]. We can make a gedanken experiment as visualized in Figure 4.24 to understand this behavior and use it to prove the minority spin of the electrons, which accounts for the dichroic excitation.

A starting point is the spin-dependent lifetime (see panel a) in Figure 4.24). In the spin-integrated measurements the sum of these two components is measured. Let us now assume that the number of majority and minority electrons which are excited into the image-potential state depends on the magnetization direction.
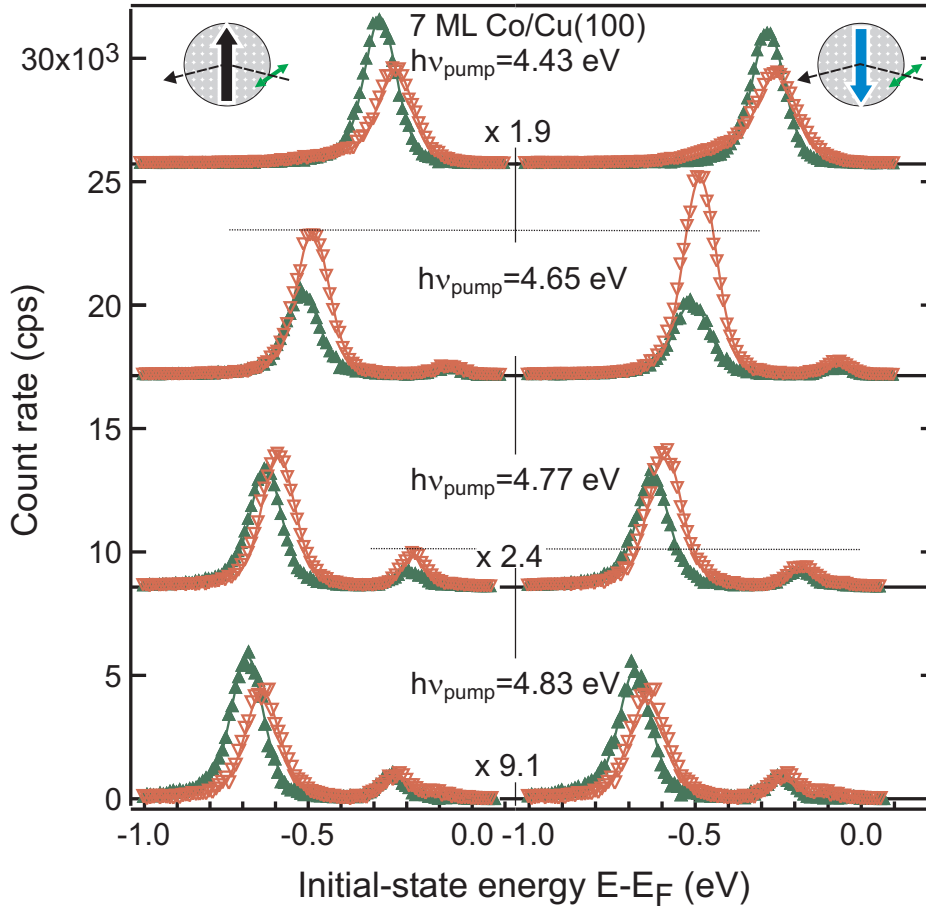
Figure 4.22: *Spin dependence of dichroic features. Spin-resolved measurements of 7 ML Co/Cu(100) plotted for the two different magnetization directions. The horizontal lines indicate the change in minority count rate.*

In the gedanken experiment we will always assume that for one magnetization direction (black curve) an equivalent number of majority and minority electrons are excited. In the other magnetization direction (blue curve) the number of excited electrons decreases by a certain, spin-dependent factor. Three scenarios are considered:

- In panel b) of Figure 4.24 we assume that the number of excited majority and minority electrons is still equivalent but by a factor of 0.6 smaller compared to the opposite magnetization direction. In this case the temporal evolution for both magnetization directions differs by this factor and results as a shift in the logarithmic plot.

- In the second scenario (Figure 4.24 panel c)) we assume a change only in the majority count-rate. At an high pump-probe delay the majority

cont rate dominates the signal since majority electrons live longer than minority electrons. Therefore the two time-resolved measurements diverge with increasing pump-probe delay.

- In the third case (Figure 4.24 panel d)) the majority intensity is independent of the magnetization direction and we only think of a change in the minority count rate. For zero pump-probe delay we have a considerable difference in the spin-integrated intensity but at a very high delay most of the minority electrons have already relaxed whereas there is still a significant amount of excited majority electrons. This implies that with increasing pump-probe delay the two time-resolved measurements converge, which is equivalent to a decreasing dichroism.

The last scenario is indeed observed for time-resolved measurements at energies where dichroism exists, two of them are plotted in Figure 4.23. Therefore even from time-resolved measurements without any spin resolution, we can deduce that the dichroism is caused by minority electrons in this experiment, which is in accordance with the results from spin-resolved measurements.

4.3.4   Dichroism in the low energy cut-off

Before discussing the microscopic origin of dichroism we have a look at the low energy cut-off. As explained in Section 4.2.2 one almost obtains equivalent information about the initial states compared to an excitation via the image-potential states. So we expect to observe the same dichroic features in the low energy cut-off as we have seen in the image-potential states at the corresponding energy of the initial states. In Figure 4.25 the low energy cut-off and the $n\geq2$ image-potential states are plotted versus the respective initial-state energy. The following facts can immediately be observed: Firstly, we indeed see strong dichroism in the low energy cut off. Secondly, the dichroism changes as a function of initial-state energy. Thirdly, the dichroism in the image-potential states and the low energy cut-off are indeed roughly at the same initial-state energy. The corresponding spin-resolved measurements in Figure 4.26 indicate a minority state which accounts for the dichroism.

This is consistent with our findings from spin-resolved measurements in Section 4.2.2. What is more, it demonstrates the feasibility to use photoelectron spectroscopy with lasers to study dichroism at or close to the Fermi level. This has already been shown for circularly polarized light on various $3d$ ferromagnets [*Nakagawa and Yokoyama*, 2006] but without any photon-energy dependence.

4.3.5   Microscopic origin of dichroism

After having presented the dichroic effects in the spin- and time-resolved 2PPE spectra we have to focus on the microscopic origin. In Section 4.2.2 we explained
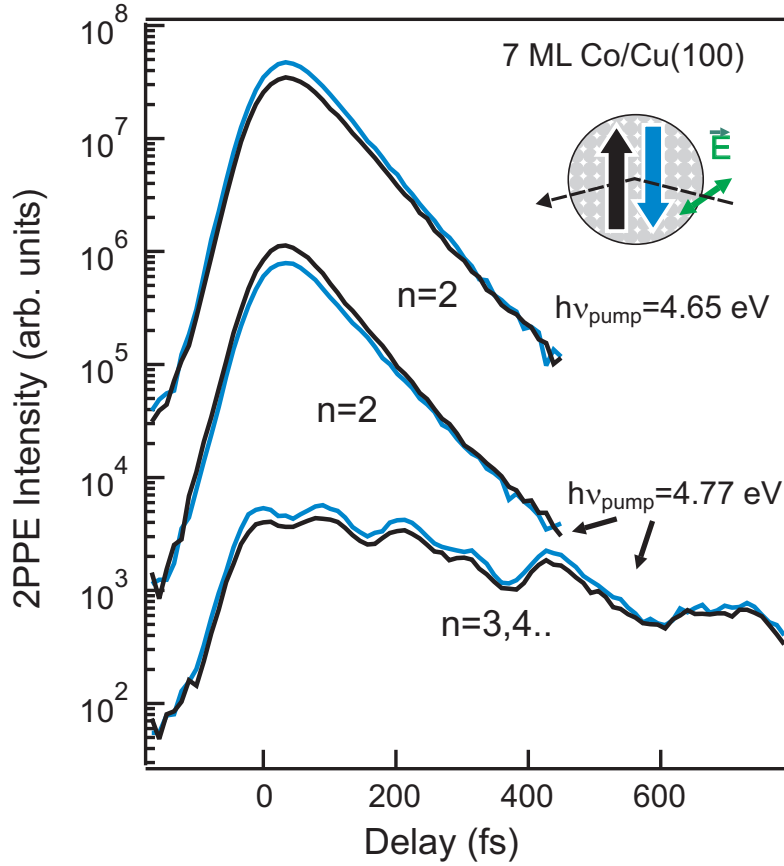
Figure 4.23: *Dichroism in time-resolved 2PPE measurements. Measurements were made for the n=2 and n≥3 state from 7 ML Co/Cu(100) for two different magnetization directions. The pump-pulse photon energy was 4.65 eV and 4.77 eV, respectively. In all cases the dichroism vanishes with increasing pump-probe delay.*

the possible transitions by using a band structure (see Figure 4.9), however, only in the non-relativistic limit, where spin-orbit coupling is neglected. This means that the representation of the states is solely determined by the crystal symmetry. The point group is C_{4v} in the case of states lying along the Δ direction. The spin space is completely decoupled and therefore the spin quantum number can be separated from the symmetry quantum number.

Taking now spin-orbit coupling into account, spin and spatial quantum numbers can no longer be treated independently. The electronic states are determined by new representations due to the formed double group **DG**, which is a direct product of the single group with the rotational group of spin space **DG** = **G** $\otimes$ **SU₂**. This leads to a lowering in symmetry, and therefore also diminishes the set of irreducible representations. For states along the Δ direction we are left with two new representations Δ_6 and Δ_7, which emerge from
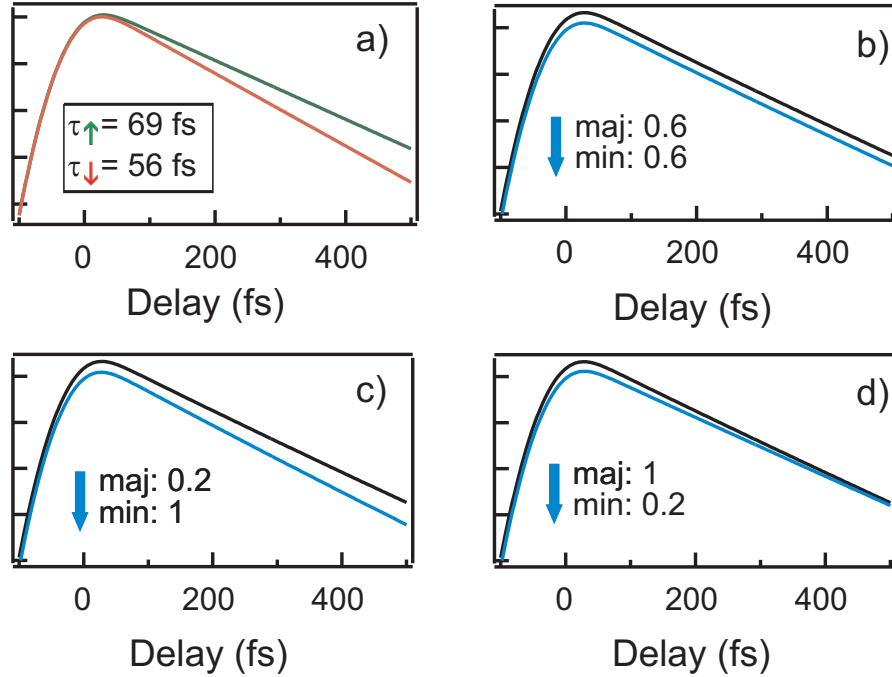
Figure 4.24: *Explanation of 'dichroic' lifetime by a gedanken experiment. In panel a) the spin-dependent lifetimes are visualized in a spin-resolved 2PPE spectrum. In panel b)-d) three different scenarios for the dichroic time-resolved measurements are considered. In panel b) a general lower count rate with a factor of 0.6 is assumed for the measurement in one magnetization direction (indicated by the blue arrow). In panel c) only a reduction of the majority count rate and in panel d) of the minority count rate is considered. At a high pump-probe delay one obtains a completely different behavior for each scenario.*

the former point group representations. The inclusion of a magnetization vector lifts time-reversal symmetry and, in the case of an *in-plane* magnetization along a high symmetry axis, two one dimensional representations exist (γ_1 and γ_2), which transform into each other by the time-reversal operator [*Henk et al.*, 1995]. There is still a connection between the former spatial and spin quantum numbers and the new representations (see e.g. [*Kuch and Schneider*, 2000]):

$$\Delta_{1\uparrow}, \Delta_{1'\downarrow}, \Delta_{2\downarrow}, \Delta_{2'\uparrow}, \Delta_{5\uparrow}, \Delta_{5\downarrow} \longrightarrow \gamma_+$$
$$\Delta_{1\downarrow}, \Delta_{1'\uparrow}, \Delta_{2\uparrow}, \Delta_{2'\downarrow}, \Delta_{5\uparrow}, \Delta_{5\downarrow} \longrightarrow \gamma_-$$

$$(4.3)$$

where $\uparrow$ and $\downarrow$ denote the majority and minority state. In the case of vanishing spin-orbit coupling the representation of the states converge to the spatial and spin representation.

The band structure in Figure 4.27 a) accounts now for the new representations. The yellow circles mark the crossing points of bands with equal symmetry. The states hybridize at these points, which results in a splitting in energy. This is now
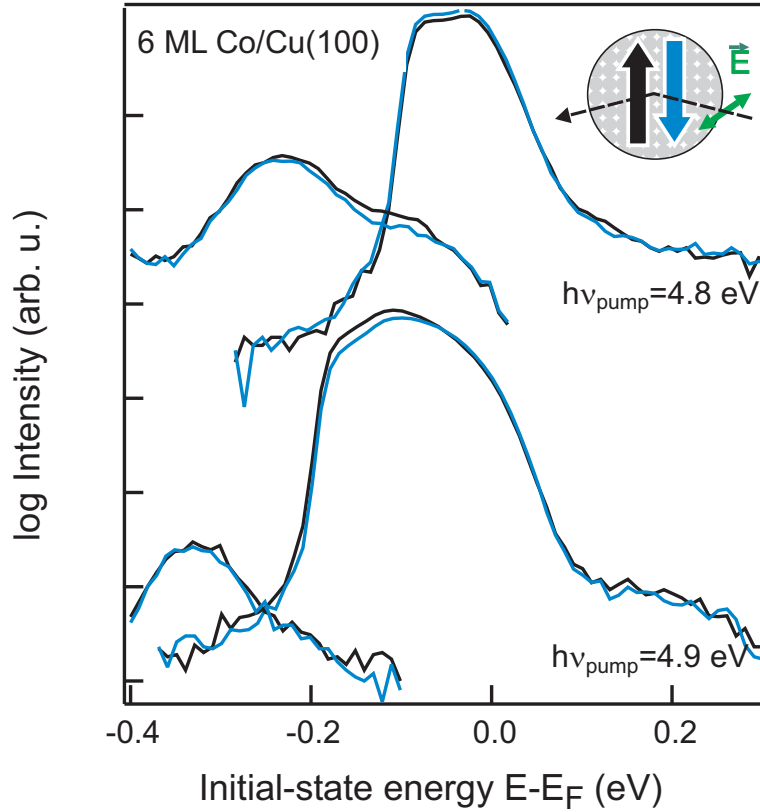
Figure 4.25: *Dichroism of the low energy cut-off for 6 ML Co/Cu(100). As a comparison the dichroism of the n=2 and n=3 state are included at the corresponding initial-state energy.*

considered in 4.27 b) where these so-called avoided crossings are schematically drawn into the band structure. Due to the hybridization a superposition of the former spatial part of the wave functions as well as their spin is obtained. It will turn out later that these points of large hybridization play the crucial role in magnetic linear dichroism.

The measure in photoemission spectroscopy, the photocurrent, is determined by the dipole selection rules, which still depends on the spatial symmetry of the initial and final states as in the case of vanishing spin-orbit coupling. With p-polarized light one can excite states with a Δ_1 and a Δ_5 representation into a final state with Δ_1 symmetry. This depends on the perpendicular ($A_\perp$) and parallel ($A_\parallel$) component of the vector potential and thus on the angle of incidence as explained in Section 2.3.2. By neglecting spin-orbit coupling the transitions from the Δ_1 and Δ_5 state can be treated separately. However, considering spin-orbit coupling and focusing on the states with strong hybridization between states with a Δ_1 and a Δ_5 symmetry an additional interference term has to be taken into account. This is explicitly calculated in [*Henk et al.*, 1995] for an arbitrary
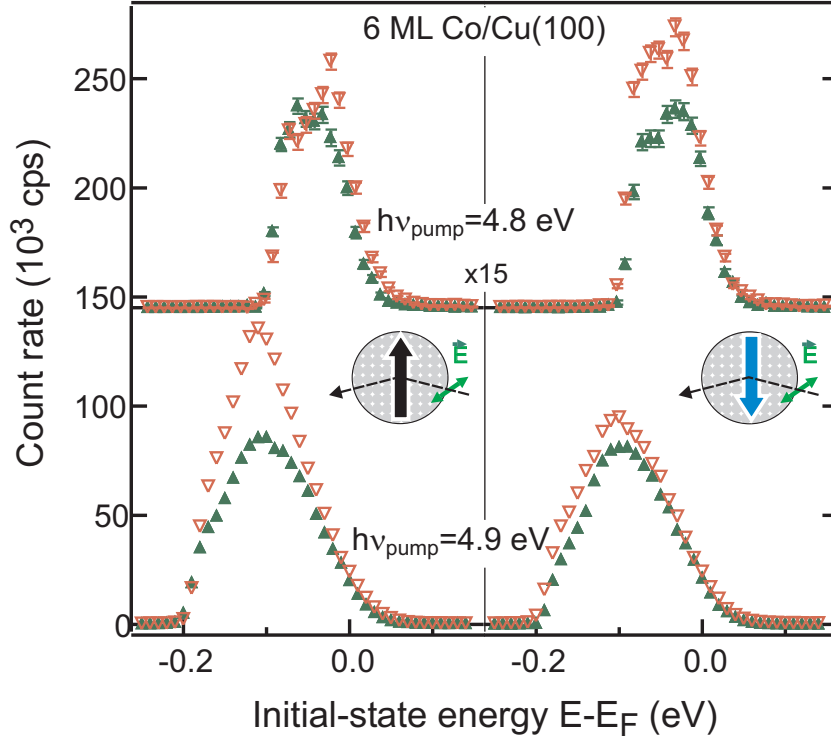
Figure 4.26: *Minority effect of dichroic features in the low energy cut-off. The data from Figure 4.25 is plotted with spin-resolution for both magnetization directions.*

angle of incidence. For the sake of clarity we will, however, refer to the simplified formula for the photoemission current given in [*Kuch and Schneider*, 2000] for a measurement geometry similar to the present one:

$$
\begin{aligned}
I(\mathbf{M}\pm) =&(\sin^2\vartheta)(|M^{1++}|^2 + |M^{1--}|^2) + (\cos^2\vartheta)(|M^{5++}|^2 + |M^{5--}|^2) \\
&\pm (\sin\vartheta)(\cos\vartheta)\Im(M^{1++*}M^{5++} - M^{1--*}M^{5--})
\end{aligned}
\tag{4.4}
$$

For the final state always a Δ_1 spatial symmetry is assumed, the spatial symmetry of the initial state is given in the superscript of the transition matrix elements M. The two signs refer to the representation of the initial state and final state. For example M^{5++} denotes a transition matrix element from an initial state with Δ_5 symmetry and a γ_+ representation into a final state with γ_+ representation. The incident angle with respect to the surface normal is given by ϑ. The first two terms in Equation 4.4 describe the incoherent part and the last term can be ascribed to the interference term due to emission from an initial state with both, Δ_1 and Δ_5 symmetry. The sign of the latter also depends on the sign of the magnetization $\mathbf{M}$, which leads to the observed dichroism.

Being interested in the origin of the dichroic features we focus on the interference term in the further discussion. Here the two products of the transition
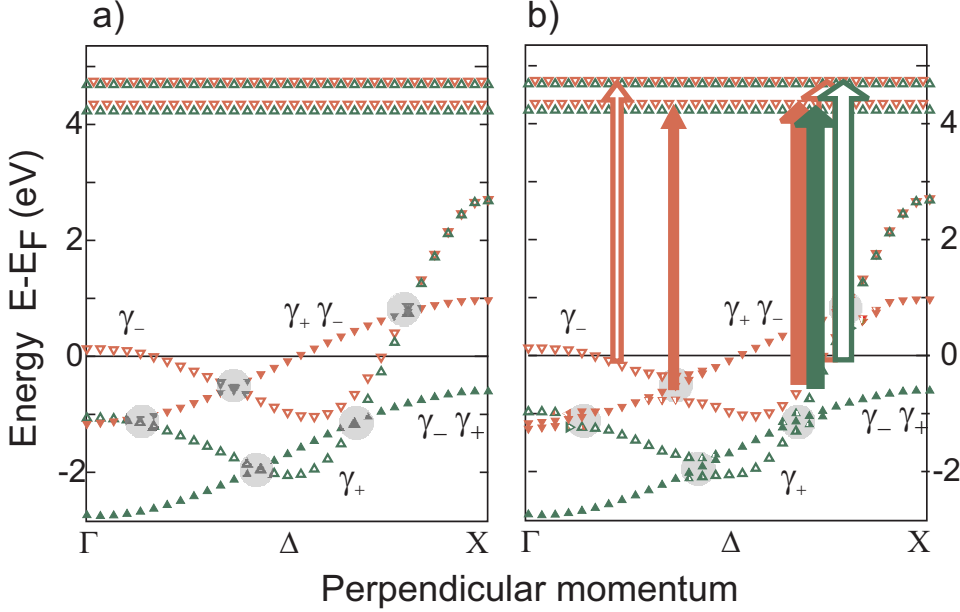
Figure 4.27: *Influence of spin-orbit coupling on the electronic band structure depicted from Figure 4.9. a) With relativistic quantum numbers. The former 2-dimensional Δ_5 band is split in a γ_+ and a γ_- band, which energy difference is small compared to the exchange splitting and neglected in this schematic. b) Including hybridization and possible excitations to the image-potential states.*

matrix elements in the interference term, namely $M^{1++*}M^{5++}$ and $M^{1--*}M^{5--}$ have to be examined. The final states are in this experiment the image-potential states[4]. They have Δ_1 symmetry and according to the assignment in 4.3 their representation is given by γ_+ for the majority states and γ_- for the minority states. Since we mainly observe dichroic features in the minority image-potential states, whose relativistic quantum number is γ_- , only the product $M^{1--*}M^{5--}$ in Equation 4.4 contributes to the interference term. In these matrix elements also the initial states have a γ_- representation. Therefore, we can conclude that the *dichroism is caused by γ_- states* which have Δ_1 and Δ_5 symmetry.

We may now turn back to panel b) in Figure 4.27 to explain the dichroism in our spectra by a simple band structure where spin-orbit coupling is included. A possible candidate for dichroism are the two γ_- bands, one with Δ_1 and the other with Δ_5 symmetry which hybridize at about $E - E_F = -0.5$ eV below the Fermi level halfway between Γ and X. The hybridization causes an avoided crossing of the bands and leads to a gap which should result in two dichroic features in a photoemission spectrum. This has already been observed in ultraviolet photoemission spectroscopy [*Fanelsa et al.*, 1996]. It is not clear which of the three dichroic features can ascribed to this avoided crossing. Comparison to data in

---

[4]The probe-process is completely disregarded

[*Fanelsa et al.*, 1996], especially concerning the sign of the dichroism suggests that the two dichroic features at $E - E_F$ =-0.18 eV and -0.05 eV in Figure 4.21 would be good candidates so far. The strong dichroism at $E - E_F$ =-0.45 eV could be explained by the existence of a hybridization of the band bottom of the Δ_1 minority band with the Δ_5 minority band by this simple model.

However, combining our findings from the dichroic and spin-resolved measurements it becomes obvious that the minority surface resonance derived in Section 4.2.2 energetically exactly coincidences with the strong dichroism at $E - E_F = $ -0.45 eV. Therefore, we can conclude that this surface resonance leads to dichroism in photoelectron spectroscopy.

4.3.6   Thickness dependence

Although an explanation for the three dichroic features was given in the previous subsection some more information has to be presented. One might have already realized that the spectra were recorded for different film thickness. Dichroism was observed in all spectra, however with some difference with respect to the initial-state binding energy. The energetic positions for the maxima of asymmetry are plotted versus the thickness in Figure 4.28. It can clearly be seen that the dichroic feature, which we assigned to a surface resonance is independent of coverage, but the features slightly below the Fermi level show a thickness dependence.
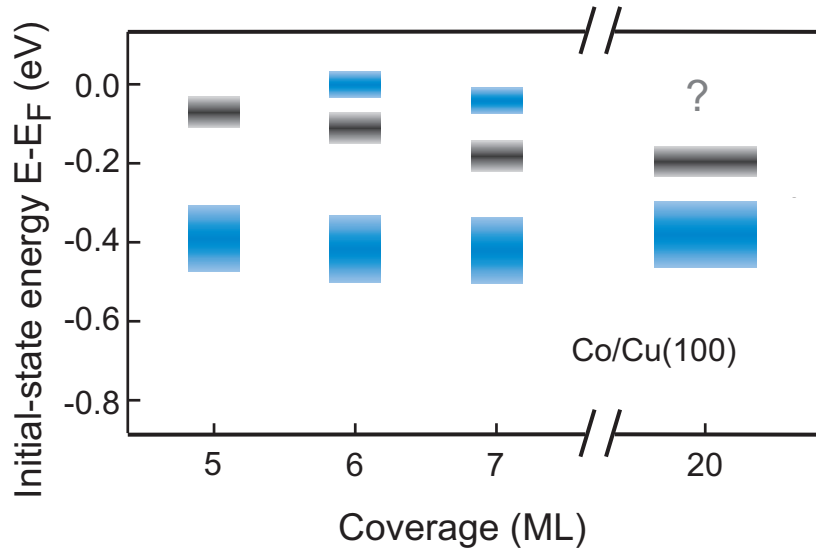
Figure 4.28: *Coverage dependence of the asymmetry. The color corresponds to the sign of the asymmetry (*blue* corresponds to positive, black to negative asymmetry in our definition). For a coverage of 20 ML, no data is available to initial state energies, close to the Fermi level, which is indicated by a question mark.*

The thickness dependence could now only be justified by a shift of the Δ_5

band with coverage, which also leads to a shift of the avoided crossing. Indeed, *Schneider et al.* [1991a] observed an upward moving of the minority Δ_5-type band with thickness, which was ascribed to a decreasing compression of the film in the axis perpendicular to the surface. The upward movement of the Δ_5 band would however also result in an upward shift of the avoided crossing and therefore also of the dichroic features. However, the opposite behavior was observed (see Figure 4.28).

Since the coverage is in the range of only a few atomic layers quantum-size effects might explain this thickness dependence. Especially quantum confinement of electrons in thin films, known by the term quantum-well states, have attracted considerable interest in some cases due to its connection to giant magneto resistance (see e.g. [*Bürgler and Grünberg*, 2005]).

Their existence is based on a confinement of the electrons in the film at the specific binding energy. The boundary is caused by the different electronic band structure of the film and the substrate. This allows states to exist in a specific energy range in the film but not in the substrate.[5]

Quantum-well states have extensively been studied for Cu/Co(100) films, (see e.g. [*Ortega and Himpsel*, 1992, *Segovia et al.*, 1996]), especially due to their connection with exchange coupling in Co/Cu/Co triple layer systems [*Bloemen et al.*, 1994]. However, little is known about quantum-well states on Co/Cu(100). Inverse-photoemission studies observe quantum-well states and resonances at binding energies well above the Fermi level [*Ortega et al.*, 1993, *Yu et al.*, 2003], which is also in accordance to *ab initio* calculations [*van Gelderen et al.*, 1996].

Around the Fermi level in fcc Co(100) majority and minority states exists with Δ_1 symmetry. In contrast, states with Δ_5 symmetry have a minority spin (see Figure 4.9). In Cu (100) we have only states with a Δ_1 symmetry at this energy range (not shown). Therefore, we may only expect minority quantum-well states with a Δ_5 symmetry [*Pérez-Díaz and Muñoz*, 1996]. These quantum-well states can hybridize with the Δ_1 band, which should be observable in dichroic measurements, as observed in this experiment. More experimental data for other film thickness are needed to support this assumption. So far direct photoemission did not show any evidence for quantum-well states below the Fermi level of Co/Cu(100) [*Schneider et al.*, 1991a, *Clemens et al.*, 1992a].

---

[5]In case the film states can couple to the substrate one would speak of quantum-well resonances.

4.4 Photoelectron spectroscopy via observer states

To finish this chapter the results have to be critically reviewed. We have shown that spin-resolved 2PPE via image-potential states can be used to study the electronic structure of ferromagnets with respect to the following properties.

- *Energy:* The possibility to tune the wavelength of the pump pulse gives us access to states in an energy range between $E - E_F$ = -0.8 eV and the Fermi level. It has to be noted that the sensitivity to initial states is limited to specific energies for one measurement. By exciting via the $n=1$, $n=2$ and $n=3$ state we have probed at three energies. To collect data from other energetic positions in the electronic structure the photon energy of the laser has to be tuned. Furthermore, laser parameters like power and pulse width considerably change between measurements with different photon energies, which affects the overall count rate. Nevertheless, the influence of the initial-state density and its surface character on the intensity in the spectrum is observable. Vice versa the spectra can be used to identify surface resonances and gaps in the electronic structure.

- *Spin:* The spin-polarization detector provides a spin sensitivity in the *in-plane* and *out-of-plane* direction. Due to the spin-dependent dynamics of the image-potential-state electrons the original spin-polarization is modified. This can, however, easily be corrected afterwards since the dynamics can be determined by time-resolved measurements.

- *Symmetry:* The possibility to switch the pump-pulse between p- and s-polarization in combination with the dipole selection rule gives access to states with different symmetry. In the present case (fcc crystal with a (100) surface) we are able to distinguish between with Δ_5 and Δ_1 representation.

- *Hybridization:* The observation of dichroism proved that one is able to detect electronic states which inhibit a mixing of two different spatial symmetry quantum numbers. The mixing is due to spin-orbit coupling which causes two states with different spatial symmetry to hybridize. The feasibility of a spin-resolved detection or time-resolved spectroscopy via image-potential states even allows one to assign a spin character to these hybridized states.

- *Surface sensitivity:* Due to the small penetration depth of the image-potential states into the bulk this technique is very surface sensitive. The surface character of the image-potential states also facilitates data interpretation since one has not to worry about a spin-filter effect [*Kuch et al.*,

1995] due to a spin-dependent transport in the excitation process. An inelastic background signal can therefore also be neglected. Furthermore, due to the small overlap of the image-potential states with the bulk, spin orbit coupling is negligible. Only for high-Z elements spin-orbit coupling in the image-potential states is expected to be measurable [*McLaughlan et al.*, 2004]. Therefore image-potential states do not cause any dichroism.

The surface sensitivity was also proved for the electrons which were directly excited by the pump-pulse into the final state.

Furthermore, the present experimental set-up provides the possibility to vary the electron emission angle, which gives access to states with $k_{\parallel} \neq 0$. Additionally, the angle of incidence of the laser beam can be changed by selecting a different entrance window of the UHV-chamber. This could be used to study magnetic linear dichroism in more detail or spin-polarized excitation in paramagnetic materials.

One has again to remember that 2PPE is designed to study the electronic structure and dynamics of unoccupied states. The possibility to combine all these results in one experiment can be regarded as an outstanding opportunity.